

First derivatives at the optimum analysis (*fdao*): An approach to estimate the uncertainty in nonlinear regression involving stochastically independent variables

Carlos Sevcik*

Laboratory on Cellular Neuropharmacology, Centro de Biofísica y Bioquímica, Instituto Venezolano de Investigaciones Científicas (IVIC), Caracas, Venezuela.

Abstract

An important problem of optimization analysis surges when parameters such as $\{\theta_j\}_{j=1,\dots,k}$, determining a function $y = f(x \mid \{\theta_j\})$, must be estimated from a set of observables $\{x_i, y_i\}_{i=1,\dots,m}$. Where $\{x_i\}$ are independent variables assumed to be uncertainty-free. It is known that analytical solutions are possible if $y = f(x \mid \theta_j)$ is a linear combination of $\{\theta_{j=1,\dots,k}\}$. Here it is proposed that determining the uncertainty of parameters that are not *linearly independent* may be achieved from derivatives $\frac{\partial f(x \mid \{\theta_j\})}{\partial \theta_j}$ at an optimum, if the parameters are *stochastically independent*.

Keywords: Stochastic independence, Data ratios, Cauchy distribution, Hill equation, Boltzmann equation.

1. Introduction

An important problem of optimization analysis surges when it is desired to guess the parameters $\{\theta_{i=1,\dots,k}\}$, determining a function $y = f(x \mid \{\theta_{i=1,\dots,k}\})$ (also called the *objective function*, *obf*) must be determined from a set of observables $\{x_j, y_j\}_{j=1,\dots,m}$. Where $\{x\}$ are independent variates assumed to be uncertainty-free (called explanatory variables), and their associated observed dependent variates (response variables), $\{y\}$. Analytical solutions are possible, and many are well known (see for example [1]), when $f(x \mid \{\theta\})$ involves a linear combination of $\{\theta\}$. In the case of nonlinearly independent [2, 3] $\{x_i, y_i\}$ pairs:

“In general, there is no closed-form expression for the best-fitting parameters, as there is in linear regression. Usually numerical optimization algorithms are applied to determine the best-fitting parameters. Again in contrast to linear regression, there may be many local minima of the function to be optimized and even the global minimum may produce a biased estimate. In practice, estimated values of the parameters are used, in conjunction with the optimization algorithm, to attempt to find the global minimum of a sum of squares ”.

*Prof. Carlos Sevcik, IVIC CBB, Apartado 20632, Caracas 1020A, Venezuela. Email: csevcik@ivic.gob.ve. Business Email: carlos.sevcik@scimedan.com, web page: www.scimedan.net

The problem of local minima is inherent to the function fitted and cannot be avoided. Yet, efficient minimization algorithms, which start searching from a set of user provided $\{\theta_i\}_{init}$ parameters in case of many “well behaved functions” converge towards the global optimum if $\{\theta_i\}_{init}$ is within a certain boundary of the global optimum $\{\theta\}_{opt}$. There is, however, no analytical solution to the problem of knowing the width the boundary of guaranteed convergence to the global optimum (minimum or maximum) for a given obf.

The gradient represents the slope of the tangent of the graph of the function. More precisely, points in the direction of the greatest rate of increase or decrease of a function, and its magnitude is the slope of the graph in that direction. For an optimization process fitting data to an *obf* such as $f(x \mid \{\theta_{j=1, \dots, k}\})$ to be at an optimum, the following identity

$$f(x \mid \{\theta_{j=1, \dots, k}\}_{opt}) \iff \nabla_{\theta} = \sum_{j=1}^k \frac{\partial f(x \mid \{\theta\}_{opt})}{\partial \theta_j} = 0 \quad (1)$$

must be true (vertical bars mean ‘given that’ and all along this paper curly braces indicate sets of elements). It is usually assumed that the *obf* exactly describes the system whose optimum set of values is being determined, and that differences between model and data (called residuals) result from lack of accuracy in measuring a given y_i for x_i

Yet, data from the physical world always contains uncertainty which does not result from measurement error. The sources are many: Limitations of the observation instrument make the measurements fuzzy; optical instruments are a very intuitive example of fuzziness; actually, measuring instrument introduces fuzziness, which is dependent on the instrument’s limit of resolution; impossibility of accurately measuring something, a classical example deals with the velocity and position of a particle [4]; observing reality with a scope (aim or purpose) modifies the object observed [5], this is specially relevant to quantum physics, but applies to any measurement (draining current, compressing with a caliper, heating, etc.) to, hopefully, a minor extent; uncertainty is essential to life, otherwise any noxious factor would affect equally a whole species population making its extinction likelier, thus any parameter measured on living beings is significantly variable, uncertain, fuzzy [6]; fuzziness appears also when the object measured changes more or less cyclically in time, the height of the Mont Blanc peak (like most other mountains) is a well known case [7, 8]; since temperature (T) is $T > 0^\circ\text{K}$, molecules vibrate and rapidly change between conformations and molecular properties are fuzzy too [9–11]; in high energy physics the existence of a particle was evidenced by an energy peak which had to be differentiated from background noise [12]; all processes of chemical or electrical intercellular communication are stochastic in nature [13–16]. In all these instances observations randomly vary, not due to experimental “error” but due to the stochastic nature of the process under study by it self. This is most likely the case for processes such as the ones described with the Hill [Eq. (23)] or Boltzmann [Eq. (48)] equations, when these equations are used mechanistically, not just as curve fitting processes. The inter-molecular reaction parameters of the Hill equation are scholastically independent, the maximum effect of speed of catalysis (y_m) does not depend on the affinity constant of the reactants (K_m) and none of them depends on the molecularity of the reaction (number of molecules of one kind reacting with a molecule of another kind, n) [17–19]. A similar reasoning can be used in connection with the Boltzmann equation [Eq. (48)] where $V_{\frac{1}{2}}$ and κ are mechanistically independent. In both cases obf parameters are *causally independent*. Briefly unther these conditions we have

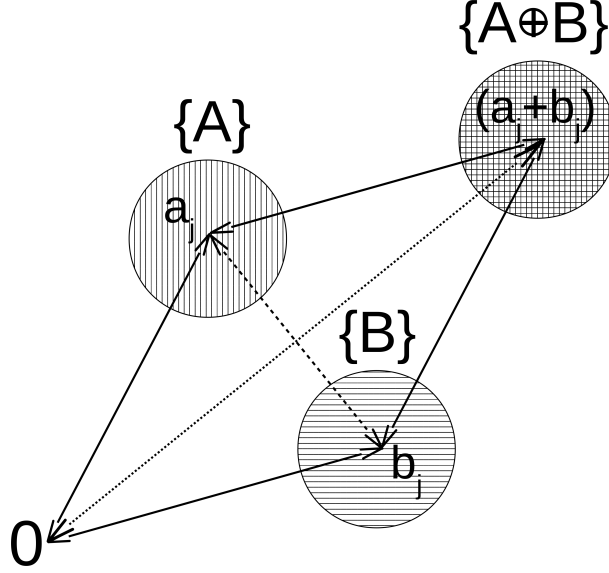


Figure 1: **Plot of the Minkowski sumset $\{A \oplus B\}$ in Eq. (3).** Dotted arrow represent $(a_j + b_j)_j$ bijection as a vector. A dashed arrow drawn to stress graphically that $\{A\}$ and $\{B\}$ are bijections one of them representing objective function parameters at the optimum, and, the other one, their inherent uncertainties. All sets in the figure have same cardinality $|A| = |B| = |A \oplus B| = k \geq j \geq 1, j \wedge k \in \mathbb{Z}$, which equals the number of parameters required by the objective function. “0”, indicates the origin of coordinates. Other details in the text of the communication.

Condition 1.

$$(\theta_l \perp\!\!\!\perp \theta_h) \forall (l \neq h) \mid \langle (\theta_l \wedge \theta_h) \in \{\theta_{j=1,2,\dots,n}\} \rangle.$$

where $\perp\!\!\!\perp$ indicates stochastic independence, the concept of *causal independence* between variables or factors [20–22], a notion which has also recently been used in fields such as quantum thermodynamics [23–25], $\perp\!\!\!\perp$ is opposite to $\not\perp\!\!\!\perp$ meaning stochastic dependence. We may write a function representing these conditions as an equation based on Eq. (1)

$$\begin{aligned} g(\{x_i\} \mid \{\tilde{\theta}\}) &= f(\{x_i\} \mid \{\psi(\mu = \theta_j, \sigma_j^2)\}_{j=1,2,\dots,k}) \\ &\dots = f(\{x_i\} \mid [\{\theta_j\} + \{\psi(0, \sigma_j^2)\}]_{j=1,2,\dots,k}). \end{aligned} \quad (2)$$

Now, $\{\tilde{\theta}\} = \{\theta_j + \psi(0, \sigma_j^2)\}_{j=1,2,\dots,k}$, is a Minkowski sum [26] of two independents sets such as

$$\{A\} \oplus \{B\} = \{a_j + b_j \mid a_j \in \{A\} \wedge b_j \in \{B\}, \{A\} \wedge \{B\} \in \mathbb{R}\}_{j=1,2,\dots,k}, \quad (3)$$

as illustrated in figure 1, Eq. (3) is a bijection for which the following holds:

$$[\forall (a_j \in \{A\}) \wedge \forall (b_j \in \{B\}) \overset{\text{b}}{\exists}_1 (a_j + b_j)_j \in \{A \oplus B\}] \mid \{A\} \wedge \{B\} \in \mathbb{R}. \quad (4)$$

In Eq. (2), $\psi(\theta_j, \sigma_j^2)$ is a random variable with mean $\mu = \theta_j$ and variance σ_j^2 . Sets $\{A\}$ and $\{B\}$, as shown in figure 1, are bijections with set $\{A\} \oplus \{B\}$. When dealing with a “pathological distribution”, such as the Cauchy *probability density function (pdf)*, whose statistical central moments are undefined (have no meaning) and thus neither its population mean nor its variance are defined

[27–29], the random component in Eq. (2) may be expressed in terms its *median* ($\widehat{\mu}_j = \theta_j$) and *scale factor* (γ_j) [Eq. (29)] to become $\psi(\theta_j, \gamma_j)$. In both cases

$$g(\{x_i\} \mid \{\tilde{\theta}\}) = f(\{x_i\} \mid \{\theta_j\})_{j=1,2,\dots,k} + f(\{x_i\} \mid \{\psi(0, \sigma_j^2)\})_{j=1,2,\dots,k} \quad (5)$$

At an optimum $\{\tilde{\theta}\}_{opt} = \{\theta_{j,opt} + \psi(0, \sigma_j^2)\}_{j=1,2,\dots,k}$ the gradient is not zero, but a function which *randomly fluctuates about zero* since its parameters fluctuate, *and the fluctuations of each parameter is independent from the other parameters* [Eq. ??]. Thus at any given $\{x_i\}_{i=1,2,\dots,m}$

$$\begin{aligned} \nabla_{x_i, \tilde{\theta}}^r &= \sum_{j=1}^k \frac{\partial g(\{x_i\} \mid \{\tilde{\theta}_{opt}\})}{\partial \tilde{\theta}_{j,opt}} \\ &\approx \sum_{j=1}^k \frac{\partial f(\{x_i\} \mid \{\psi(\tilde{\theta}_{j,opt}, \sigma_j^2)\})}{\partial \tilde{\theta}_{j,opt}} \\ &= \sum_{j=1}^k \omega(\tilde{\theta}_{j,opt}) \neq 0. \end{aligned} \quad (6)$$

Eq. (6) shows that data are variable, the *obf* is ‘fuzzy’, with a mode $\bar{g}(\{x\} \mid \{\tilde{\theta}\})$. Eq. (6) expresses that variability [30, 31] exists, on any particular pair $\{x_i, y_i\}$ where x_i exactly set, and y_i is measured accurately. Changes in $f(\{x_i\} \mid \{\tilde{\theta}_{opt}\})$ depend on $\{\tilde{\theta}_{opt}\}$ which varies each time $f(\{x_j\} \mid \{\tilde{\theta}_{opt}\})$ is measured. In contrast with ∇_{θ} in Eq. (1), the notation $\nabla_{\tilde{\theta}}^r$ is introduced in Eq. (6) to describe the gradient at the optimum produced by *obf* random changes, to distinguish it from objective function’s gradient limit

$$\lim_{\{\theta\} \rightarrow \{\theta\}_{opt}} \nabla_{\theta} = 0. \quad (7)$$

This paper proposes that the higher a partial derivative respect to $\tilde{\theta}_{j,opt}$ in Eq. (6) is, the more sensitive the *obf* is to changes in $\tilde{\theta}_{j,opt}$. The uncertainty of $\bar{g}(x_i \mid \{\tilde{\theta}_{opt}\})_{i=1,2,\dots,m}$ due to $\theta_{j,opt}$ may be estimated as

$$\{\delta_{j\cdot}\}_{i=1,2,\dots,m} = \{\delta_{j,i}\}_{i=1,2,\dots,m} = \left\{ y_i - \bar{g}(x_i \mid \{\tilde{\theta}_{j,opt}\}) \right\}_{\substack{j=1,2,\dots,k \\ i=1,2,\dots,m}} \cdot \quad (8)$$

Rearranging Eq. (6) as

$$\{\varpi(\tilde{\theta}_{j,opt})\} = \left\{ \frac{\omega(\tilde{\theta}_{j,opt})}{\nabla_{\tilde{\theta}}^r} \right\}_{j=1,2,\dots,k} \quad (9)$$

which expresses the fraction of the gradient contributed by a parameter, it becomes possible to use the gradient on parameters [Eq. (6)] together with Eq. (8), to find how much does each parameter changes for a $\delta_{j,i}$ deviation between observed and expected *obf* values.

$$\{\vartheta_{\cdot\cdot}\} = \left\{ \prod_{i=1}^m \varpi(\tilde{\theta}_{j,i}) \delta_{j,i} \right\}_{j=1,2,\dots,k}. \quad (10)$$

In this work the set $\{\vartheta_{j,i}\}$ is used to determine how much of the empirical *obf* uncertainty at an optimum is contributed by each $\tilde{\theta}_j$ parameter, and methods are presented to enable statistical comparisons between those parameters determined under different experimental conditions. For each subset

$$\{\vartheta_j\} = \{\vartheta_{j,i=1,2,\dots,m}\} \in \{\vartheta_{\cdot\cdot}\} \quad (11)$$

2. Methods

2.1. Monte Carlo random variable simulation.

To test the goodness of fitting curves to data, random data with known statistical properties were generated using Monte Carlo simulation [32]. For this purpose sets of pairs $[x_i, f(x_i)]$ were generated as

$$f^r(x_j) = f(x_j) + \epsilon_j = f(x_j) + \psi(0, \sigma^2 \vee \gamma) \quad (12)$$

where, as said, σ^2 is the variance and γ is the Cauchy pdf scale factor. Thus for population having defined mean and variance:

$$\psi[E(x), \sigma^2] = f^r(x) = \psi(\mu, \sigma^2) \quad (13)$$

When needed, Gaussian pseudo-random variables were generated using the Box and Muller [33] algorithm as modified by Press et al. [34]. Fundamental to all Monte Carlo simulations [32] is a good uniform (pseudo) random (PRNG) number generator. Data for all numerical simulations carried out in this work were produced using random numbers (r) with continuous rectangular (uniform) distribution in the closed interval $[0,1]$ or $U[0,1]$. All $U[0,1]$ were generated using the 2002/2/10 initialization-improved 623-dimensionally equidistributed uniform pseudo random number generator MT19937 algorithm [35, 36]. The generator has passed the stringent DIEHARD statistical tests [37, 38]. It uses 624 words of state per generator and is comparable in speed to other generators. It has a Mersenne prime period of $2^{19937} - 1$ ($\approx 10^{6000}$).

The MT19937 requires an initial starting value called *seed*. The seed used was a 64-bit unsigned integer obtained using the `/dev/random` Linux PRNG, which saves environmental noise from device drivers and other sources into an entropy pool. Device `/dev/random` gets temporarily blocked, and stops producing random bytes, when the entropy of the device gets low, and commences producing output again when it recovers to safe levels. No such delays were perceived during this work. Using `/dev/random` seed makes exceedingly unlikely ($P = 2^{-64} \approx 5.4 \cdot 10^{-20}$) that the same sequence, $\{r_i\}$, of $U[0,1]$ is used twice. Calculations were programmed in C++ using g++ version 5.4.0 20160609 with C++14 standards, under Linux Mint version 18.2 running on an Apple MacBook Air computer with 8 GB RAM, Intel [®] Core™ i7-4650U CPU @ 1.70 GHz \times 4 with a 500 GB disk.

2.2. Statistical procedures.

2.2.1. Fitting functions to data

Functions were adjusted to data using a simplex minimization [39]. The simplex procedure was designed to minimize differences between empirical data assumed to obey a function such as $g(\{x_{i=1,2,\dots,m}\} \mid \{\theta_{j=1,\dots,k}\})$, where $\{x_{i=1,2,\dots,m}\}$ is a set of observables, and a model function $f(\{x_{i=1,\dots,m}\} \mid \{\theta_{i=1,\dots,k}\})$. In this work the simplex was designed to minimize

$$\varepsilon_a = \sum_{i=1}^m |y_i - f(x_i \mid \{\theta_{j=1,2,\dots,k}\})|. \quad (14)$$

Differences $y_i - f(x_i \mid \{\theta_{j=1,2,\dots,k}\})$ are commonly called *residuals*. A common alternative to Eq. (14) is

$$\varepsilon_s = \sum_{i=1}^m [y_i - f(x_i \mid \{\theta_{j=1,2,\dots,k}\})]^2 \quad (15)$$

used, for example, in the so called *least squares* minimization [1]. Minimizing least squares has a bias to give unduly high weights to outliers, which may be merely an extreme manifestation of the random variability inherent in the data, but could also stem from gross deviation from a prescribed experimental procedure or to error in calculating or recording the numerical value [40]. Giving unduly weight to outlayers is avoided by using the absolute values of the deviations as done in Eq. (14).

In this work the optimization continued looping while

Condition 2. *Keep looping while*

$$\varepsilon_{stop} = \left| \frac{\varepsilon_{a_{l+1}} - \varepsilon_{a_l}}{\varepsilon_{a_l}} \right| \underset{\circlearrowleft}{\geq} 10^{-8}, \quad (16)$$

with ε_{a_l} calculated as indicated in Eq. (14).

or else until

Condition 3. *Keep looping while $l \leq 1024000$ in Eq. (16)*

was used to stop optimization, in order to prevent the algorithm from running forever. The simplex was implemented also to provide a set $\{\delta_j\}$, used to calculate the uncertainties of $\{\theta_j\}$ estimated as described in Section 3.

The simplex algorithm requires not only a set of initiation parameters, $\{\theta_j\}_{init}$, but an initial increment value, Δ_{init} , to start modifying the initial parameters. Δ_{init} is the initial fraction to increment the parameters which is subsequently modified by the algorithm as the optimization continues [39].

2.2.2. On statistical procedures utilized.

Gaussianity of data was tested with the Jarque-Bera test, which also provides data on skewness and kurtosis of data [41] and with the Shapiro-Wilks test [42]. Unless otherwise is indicated, data are presented as medians and their 95% confidence intervals (95% CI) calculated using non-parametric Moses [43] statistics. Other data are presented as medians and their 95% confidence interval calculated with the procedure of Hodges and Lehmann [43]. Statistical significance of differences was decided with Mann–Whitney (Wilcoxon) test. Multiple comparisons were done with the nonparametric Kruskal-Wallis analysis of variance. See Hollander and Wolfe [43] for all not specified details of nonparametric methods used. Statistical differences between samples were considered significant when the probability that they stem from chance was $\leq 5\%$ ($P \leq 0.05$).

2.3. Brief description of a method to determine cell apoptosis under the action of antineoplastic drugs.

2.3.1. Brief description of the colorimetric procedure to detect cell mortality.

As an example of determining the modified Hill Eq. (24) parameters data from a study on potentially anti-neoplastic compounds by fractions isolated from the marine organism *Polyclinum constellatum* [44]. The procedure is a colorimetric assay [45–47] with a compound that has a pale yellow color, but if it penetrates into living cells it is turned into dark purple–blue crystals by an enzymatic mechanism. Dark purple–blue color is indicative of cell life. Cell death is determined

measuring light absorbance [48] of one cell thick layers (called *monolayers*) in wells where the cells are seeded. A set of wells (called blank here $\{B_h\}_{h=1,2,\dots,nb}$, $nb = 10$ replicates) was pre-treated with a detergent which kills and removes the cells from the wells prior to dye addition. A second set ($\{L_h\}_{h=1,2,\dots,nd}$, $nd = 48$ replicates) of wells contained cells, exposed only to the dye used to identify living cells, without any putative cell killing fraction; the purple-blue product of the reaction in these wells is taken to represent 100% living cells. Finally, there is a number of absorbancy sets ($\{F_h\}_{h=1,2,\dots,nf}$) measured in wells with dye and various concentrations ($[D_i] = 0.01, 0.03, 0.1, 0.3$ and 1 mg/mL) of fractions under study (named FI – FV), again, the purple-blue color is proportional to the fraction of cells not killed at the concentration tested.

2.3.2. Brief description of absorbance corrections and their use for dose–response curves.

Absorbances were corrected for blank absorbance by subtraction as

$$\{L_h^*\}_{h=1,\dots,nd-nb} = \{L_h\}_{h=1,\dots,nd} - \{B_h\}_{h=1,\dots,nb} \quad (17)$$

$$\{F_h^*\}_{h=1,\dots,nf-nb} = \{F_h\}_{h=1,\dots,nf} - \{B_h\}_{h=1,\dots,nb}. \quad (18)$$

Equations (17) and (18) indicate that each element of $\{B\}$ (background absorbance) was subtracted from each measurements in the other two sets to produce two sets corrected for cell layer background absorbance (labeled with an asterisk). The colorimetric procedure establishes [45–47] that the fraction of living cells in presence of drug is linearly proportional to the ratio

$$\{p_h\}_{h=1,\dots,nf\cdot nd-nb^2} = \frac{\{F_h^*\}_{h=1,\dots,nf-nb}}{\{L_h^*\}_{h=1,\dots,nd-nb}} \quad (19)$$

thus $n_f \cdot n_d \cdot n_b^2 = 24000$ estimates of the fraction of living cells were obtained in Quintana-Hernández [44] and used for statistical processing at each fraction concentration. Drug effect, expressed as percentage of cell death was calculated as

$$\{y_i\}_{i=1,\dots,nf\cdot nd-nb^2} = 100 \cdot (1 - \{p_h\}_{h=1,\dots,nf\cdot nd-nb^2}). \quad (20)$$

The main difference between the analyses described in Eqs, (17 – 19) and analyses in the literature, is that here the data sets were processed nonparametrically with Moses statistics [43], while most authors use a parametric approach without considering the non-Gaussianity of data involving ratios such as Eq. (19).

3. Results and discussion

3.1. A challenging data set obtained with a procedure commonly used in cell biology.

The data shown in Figure 2 (taken from [44]) are effects of several fractions (FI – FV) isolated from *P. constellatum* which were able to kill cells in culture of 4T1 breast cancer cells. Apparent effects calculated with Eq. (20) are presented in the ordinate, as function of the concentration of fraction indicated in the abscissa (in mg/mL). There are several oddities in the data, the effects at some concentrations are very disperse (As indicated by the brackets representing 95% CI), and, notably at low concentrations, they indicate negative percentages of death. At the lowest concentrations even median values are slightly, but significantly, bellow zero; this could be expected if the background correction (Eqs. (17) and (18)) actually over corrects absorbance data. The large

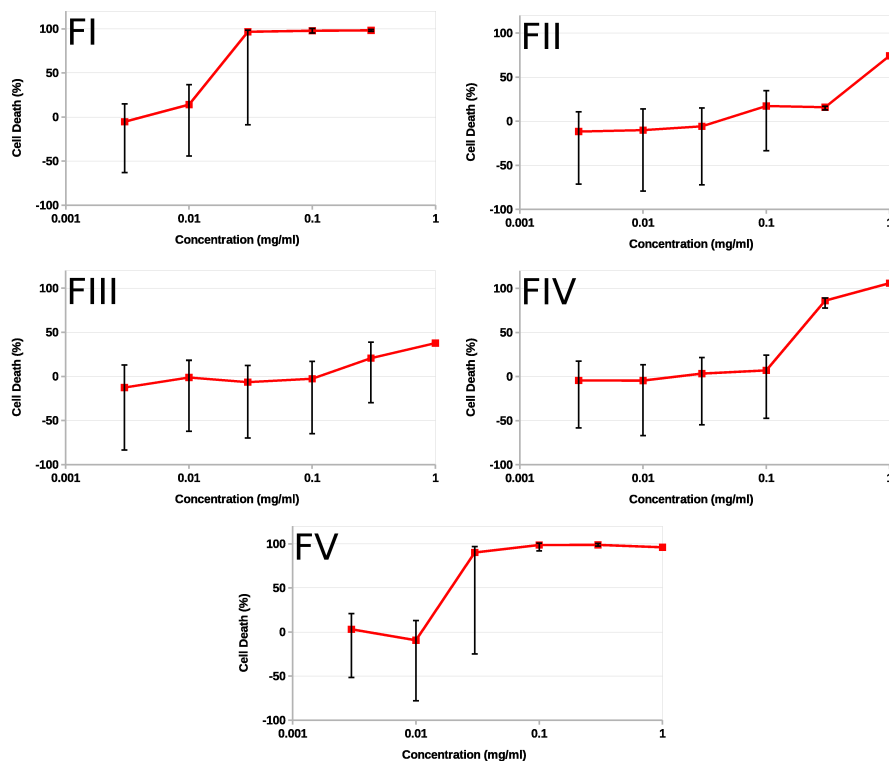


Figure 2: Cell death induced by fractions isolated from *P. constellatum* (Savigny, 1816) in 4T1 breast cancer cell cultures [44]. Percent of death calculated with Eq. (20). Ordinate is the percentage of dead cells, abscissa is concentration ([D] in mg/mL) of fraction tested, plotted in decimal logarithmic scale. Data presented as medians (■) and their 95% confidence interval (bracket lines) calculated as indicated by Hodges and Lehmann [49]. Straight lines were used to connect medians to help interpretation. The number of data processed for each fraction concentration was $n_f \cdot n_d \cdot n_b^2 = 24000$ ($n_b = 10$, $n_d = 48$, $n_f = 5$). Other details in the text of the communication

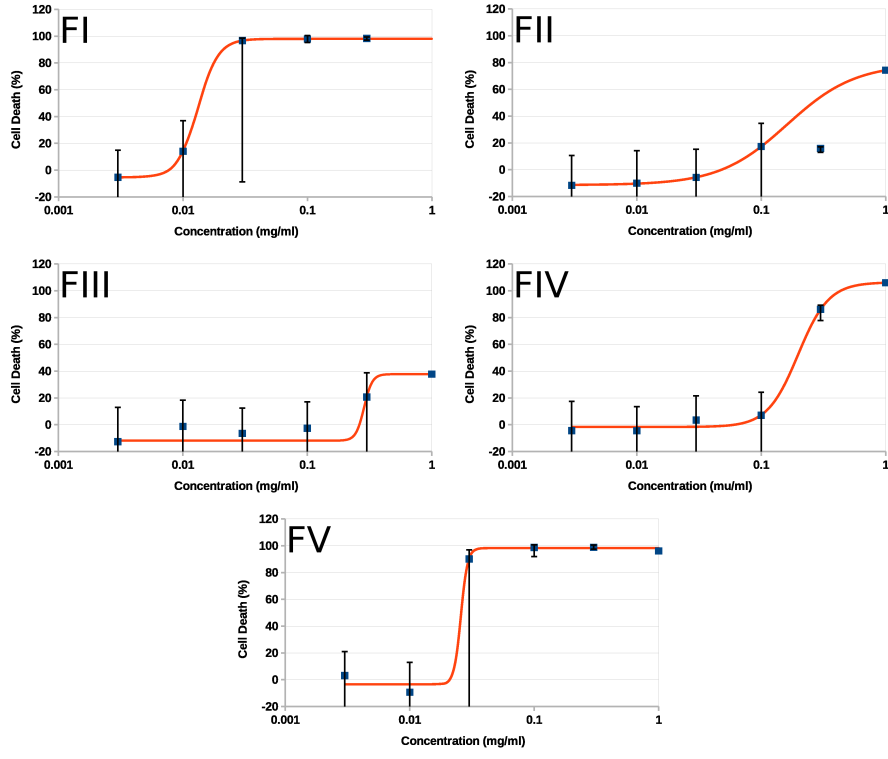


Figure 3: Cell death induced by fractions isolated from *P. constellatum* (Savigny, 1816) in 4T1 breast cancer cell cultures [44]. Ordinate was clipped at -20% to increase visibility of the biologically meaningful range of effects. All other details are equal to Figure 2 except for the sigmoid curves drawn which were calculated fitting Eq. (24) to the data with a simplex optimization procedure minimizing deviations between curves and $\{y_i\}$ data as indicated by Eq. (14). Values used to draw the curves are in Table 1. The simplex algorithm was initialized with the same set of values for the five fractions: $y_0 = -10\%$, $y_m = 100\%$, $K_m = 0.1 \text{ mg/mL}$, $n = 2$ and $\Delta_{init} = 0.1$.

Table 1: Parameters characterizing the regression curves in Figure 3.

Fraction	y_0 (%)	y_m (%)	K_m (mg/mL)	n
F1	-5.41 (-5.67, -5.16)	103.41 (103.12, 103.67)	$1.32 \cdot 10^{-2}$ (1.05, 1.56) $\cdot 10^{-2}$	5.286 (5, 284, 5.289)
FII	-11.50 (-12.34, -10.71)	90.50 (88.84, 91.95)	0.16 (0.15, 0.17)	1.59 (1.57, 1.60)
FIII	-11.92 (-13.42, -10.62)	49.67 (46.63, 52.13)	0.29 (0.27, 0.30)	13.24 (13.23, 13.27)
FIV	-1.69 (-2.06, -1.32)	108.0 (107.5, 108.5)	0.198 (0.194, 0.202)	3.525 (3.515, 3.532)
FV	-3.41 (-3.87, -3.07)	101.7 (101.2, 102.1)	$2.57 \cdot 10^{-2}$ (2.12, 2.92) $\cdot 10^{-2}$	16.165 (16.163, 16.167)

Parameters of the modified Hill Equation (24): y_0 , offset parameter; y_m , maximum effect; K_m , concentration producing half maximum effect and n , is called *Hill coefficient* or *molecularity* in some pharmacology and enzymology work [18]. The simplex algorithm was initialized with the same set of values for the five fractions: $y_0 = -10\%$, $y_m = 100\%$, $K_m = 0.1$ mg/mL and $n = 2$; Δ_{init} was set as 0.1. Please notice that the units of K_m are irrelevant as long as they are equal to the units of [D]. All data presented as medians and their 95% CI between parentheses. Confidence intervals calculated with the Hodges and Lehman [49] procedure based on data determined as indicated in relation with Eqs. (28). Sizes (m) of $\{d_{j,i}\}_{i=1,\dots,m}$ were: F1, $m = 81121$; FII $m = 96018$; FIII, $m = 114720$; FIV, $m = 115200$ and FV, $m = 114721$. Differences in m were due to sample sizes and data peculiarities due to which Eq. (19) and Eq. (28) produced undefined values called *NaN* (Not a Number, such as $\frac{0}{0}$ or $\sqrt{-x} \mid x \in \mathbb{R}$) in C++ or in values such as $\frac{x}{0}$ or $\log(0)$ called *inf* in C++. *NaN* and *inf* results were eliminated from the calculations. Other details in the text of the communication.

variability is most likely a result of subtractive cancellation [50–52], combined with the quotient represented by Eq. (19) which is prone to produce a large variance increase in $\{p_h\}$ [Eq. (19)] and $\{y_i\}$ (Eq. (20)). These problems are overlooked in cell biology literature.

Gaussianity tests indicated that all data set in the figures were apparently very much leptokurtic and were apparently strongly skewed. The Jarque-Bera test [41] (based on data skewedness and kurtosis) indicated that the probability that data sets in the figures were Gaussian is $P < 10^{-6}$. The Shaarepiro-Wilk test [42] indicated the same low probability of Gaussianity ($P < 10^{-6}$).

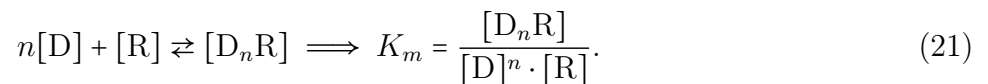
3.1.1. An example using a modified Hill equation.

The three papers describing the colorimetric method [46–48] have been cited at least 47278 times in the literature (July 22, 2017, source: <https://scholar.google.com>). This indicating that in spite of its management of uncertainty, the method has been found useful by a substantial number of researchers.

Notwithstanding the oddities of data in Figure 2, there are several features which are evidenced by the medians. All five fractions increased cell mortality as concentration raised, and in all cases there is a sigmoid aspect of the dose–effect plots.

Regression analysis [53] helps one to understand how does the dependent variable changes when the independent variable varies. Most commonly, regression analysis estimates the conditional expectation of the dependent variable given the independent variables, that is, the average value of the dependent variable when the independent variables are fixed.

The first example on how to use the theory expressed by Eqs. (??) though (11) is the analysis of a modified Hill [54, 55] equation. When the Hill equation is plotted as effect versus the logarithm o the concentration it is a sigmoid curve. In classical form, the Hill equation is used in enzyme kinetics and in pharmacology to represent the interaction of one or more molecules of subtrate with the catalytic site of an enzyme, or of a drug molecule with its receptor site is related to the the law of mass action [17–19]:



From Eq, (21), when the effect produced by drug D binding receptor R is

$$y \propto [D_nR] \implies y = \frac{y_m}{1 + (K_m/[D])^n} \quad n \in \mathbb{Z}. \quad (22)$$

Under these conditions n is called the *molecularity* of the reaction. Also, n is used in situations where properties of the enzyme or drug receptor are modified during the interaction, the, so called, cooperative schemes, where $n \in \mathbb{R}$ is plainly named *Hill coefficient* without further molecularity implications [18, 56, 57].

The Hill equation [55] in its original form is

$$y([D] \mid \{\theta_{j=1,2,3}\} = \{y_m, K_m, n\}) = \frac{y_m}{1 + \left(\frac{K_m}{[D]}\right)^n} \quad (23)$$

which does not include a term for “offset,” occurring when $y([D] = 0 \mid \{y_m, K_m, n\}) \neq 0$. Since the data in the figures seems to include an overcorrection for the basal absorbance, this modified

Hill equation will be used. as a particular case, in our analysis:

$$y([D] | \{\theta_{j=1, \dots, 4}\} = \{y_0, y_m, K_m, n\}) = y_0 + \frac{y_m}{1 + \left(\frac{K_m}{[D]}\right)^n} \quad (24)$$

its first derivatives on $\{\theta_j\}$ are given in Section B.1 as Eqs. (40) – (43).

Figure (3) shows the results of adjusting Eq. (24) to the data of Quintana-Hernández [44]. In all cases the simplex optimization started from the same set of values: $y_0 = -10\%$, $y_m = 100\%$, $K_m = 0.1$ mg/mL, $n = 2$ and $\Delta_{init} = 0.1$. Since Eqs. (17 – 19) produce 24000 points per concentration, the number of pairs in each fraction’s regression analysis ranged 120000 – 144000 in the plots shown in Fig. 3. Interestingly, the curves in Fig. 3 follow, rather closely, the median percent of dead cells at each concentration in all the plots. This is particularly clear for FI and FV. The parameter values describing the curves are in Table 1. The curves in Figure 3, and the sets of data in Table 1 “look good” but uncertainty estimator for the parameters are necessary to properly state which fraction effect differs from which fractions, specially if the outliers suggested by the 95% CI and “skewness” analysis are considered.

If the $\{\theta_j\}$ are stochastically independent [expressed $\{\tilde{\theta}_j\}$ in Eq. (2)] [20–22], Eq. (6), in finite differences [58] form, becomes

$$\omega(\tilde{\theta}_j)_i \approx \frac{\Delta f(x_i | \{\tilde{\theta}_j\})}{\Delta \tilde{\theta}_j(x_i)} \quad (25)$$

from which it follows that

$$\Delta \tilde{\theta}_j(x_i) \approx \frac{\Delta f(x_i | \{\tilde{\theta}_j\})}{\omega(\tilde{\theta}_j)_i}. \quad (26)$$

here $\Delta \tilde{\theta}_j(x_i)$ is the finite difference estimate of $\partial \theta_j$ obtained from the information available at x_i . In Eq. (26)

$$\Delta f(x_i | \{\tilde{\theta}_j\}) = f(x_i | \{\tilde{\theta}_j\}) - y_i \quad (27)$$

are estimates of residuals. So calculating sets of finite differences such as

$$\{d_{j,i}\}_{i=1,2, \dots, m} = \{\Delta \tilde{\theta}_j(x_i)\}_{i=1,2, \dots, m} \approx \left\{ \frac{f(x_i | \{\tilde{\theta}_j\}) - y_i}{\omega(\tilde{\theta}_j)_i} \right\}_{i=1,2, \dots, m}. \quad (28)$$

is a way to develop a statistic to gauge the uncertainty of $\tilde{\theta}_i$ estimates under different conditions. Medians and their 95% CIs of Quintana-Hernández’s compounds [44] $\{d_{j,i}\}_{i=1,2, \dots, m}$ sets are presented in Table 1. All $\{d_{j,i}\}_{i=1,2, \dots, m}$ sets used to guess residuals in Table 1 were tested for Gaussianity with the Shapiro-Wilk and Jarque-Bera methods, and both procedures predicted a probability $P < 10^{-6}$ that any of the sets is Gaussian.

3.1.2. An insight on the complexity of the data used for this example

Table 2 presents data on the number of iterations required by the simplex algorithm to converge to the optimum reaching Condition 2. The only exception is data for FIV, which after 1024007 (number labeled with an asterisk in the table) loops, was still unable to reach Condition 2 and after ≈ 3 h of iterations (in the author’s computer) the process was stopped after reaching Condition 3.

Table 2: Parameters characterizing the $\{d_{j,i}\}_{i=1,2, \dots, m}$ sets used to calculate parameter uncertainty in Table 1. Δ_{init} was set as 0.1.

Fraction	Loops	Parameter	Sk	Ku	Range
FI	2867	y_0	-3.95	11.5	-1.49, 0.21
		y_m	-6.30	75.5	$-1.9 \cdot 10^3, 6 \cdot 10^2$
		K_m	-2.95	11.5	-1.43, 0.28
		n	-2.95	11.5	3.9, 5.6
FII	1328	y_0	-2.90	49.1	-5.7, 0.3
		y_m	-5.66	66.8	-492, 145
		K_m	-2.90	49.1	-5.38, 0.62
		n	-2.57	40.3	-3.9, 2.0
FIII	13277	y_0	-0.87	27.42	-695, 697
		y_m	-4.35	67.5	$(-10^{26}, 5 \cdot 10^{25})$
		K_m	-0.87	27.4	-695, 697
		n	-0.70	23.1	-681.6, 710.4
FIV	1024007*	y_0	-2.48	15.04	
		y_m	-6.56	73.6	$(-2 \cdot 10^6, 5 \cdot 10^5)$
		K_m	-2.48	15.0	-0.68, 0.47
		n	-2.20	12.4	2.6, 3.8
FV	21432	y_0	-3.85	18.1	-1.6, 0.24
		y_m	-2.79	60.0	$(-7 \cdot 10^{14}, 3 \cdot 10^{14})$
		K_m	-3.85	18.1	-1.6, 0.3
		n	-3.46	14.9	14.6, 16.4

Parameters of the modified Hill Equation (24): y_0 , offset parameter; y_m , maximum effect; K_m , concentration producing half maximum effect, n , is called Hill constant; Ku , kurtosis and Sk , skewness. *Range*, *skewness* and *kurtosis* have the usual statistical meanings. *Loop*, indicates the number of times a parameter was changed during the simplex optimization [39]. For fractions I, II, III and V optimization stopped when when Condition 2 was fulfilled. In case of FIV the optimization was topped fulfilling Condition 3 after 3 h attempting unsuccessfully to fulfill Condition 2. See the text for further discussion.

The table also presents some statistical properties of the $\{d_{j,i}\}$ sets used to calculate the uncertainty of the parameters characterizing curves fitted to data in Figure 3.

The data in the table indicates that in all cases presented $\{d_{j,i}\}$ sets are highly leptokurtic and very skewed, and in some cases (as indicated by the ranges presented at the leftmost column of the table), very wide ranges indicated that extreme values were observed. These extreme values are in all likelihood due to subtractive cancellation in Eqs. (17) and (18) combined with division by very small numbers in Eq. (19) and by the nature of the distribution of ratios *per se* (see Section 3.2.1). Interestingly, most data points seem closely packed around the median value, since the 95% CI of the medians are narrow.

Table 6 presents Monte Carlo simulation of Gaussian random data distributed about Eq. (24). Data was calculated setting the concentration term at the following values (in arbitrary units): 0.001, 0.003, 0.01, 0.03, 0.1, 0.3 and 1. The number of replicates were simulated for each concentration were: 3, 10, 100 and 2000.

3.2. Monte Carlo simulation of data described by Hill's equation modified as in Eq. (24).

3.2.1. Fitting Cauchy-distributed data to the modified Hill equation.

The analysis based on the data of Quintana-Hernández [44] suggests that using the first derivatives of the objective function may produce confidence limits for stochastically independent parameters obtained from non-linear regressions. Yet, to simulate this kind of data with Monte Carlo methods faces an important problem. The quotient of two Gaussian random variables having $\mu = 0$ and variance $\sigma^2 = 1$, the standard normal probability density function $N(0, 1)$, is distributed following the Cauchy distribution (also called Lorentz, Cauchy-Lorentz or Breit–Wigner distribution) [27–29] which has a pdf

$$c(x \mid \{\gamma, \hat{\mu}\}) = \frac{1}{\pi} \cdot \frac{\gamma}{\gamma^2 + (x - \hat{\mu})^2} \quad (29)$$

where $(x, \hat{\mu}, \gamma) \in \mathbb{R}$ and $\gamma > 0$. The probability distribution function (*PDF*) is

$$C(x \mid \{\gamma, \hat{\mu}\}) = \frac{1}{\pi} \cdot \arctan\left(\frac{x - \hat{\mu}}{\gamma}\right) + \frac{1}{2}, \quad (30)$$

$\hat{\mu}$ is the *median and mode* of the distribution, and the distribution is symmetric about $\hat{\mu}$. The maximum value or amplitude of the Cauchy pdf is $\frac{1}{\pi\gamma}$, located at $x = \hat{\mu}$, γ is called the *scale factor*. Using Eq. (30), it is easy to calculate the probability $C[x \in (\hat{\mu} \pm \underline{1}\gamma) \mid \{\gamma, \hat{\mu}\}] = 0.5$, thus $\hat{\mu} \pm \underline{1}\gamma$ is the 50% CI of $\hat{\mu}$, the 69% CI (like the CI $\mu \pm \underline{1}\sigma$ in Gaussian statistics) is $\hat{\mu} \pm \underline{1.89}\gamma$. The broadness the Cauchy distribution “shoulders” becomes dramatically clear when a 95% CI is desired, since this interval is approximately $\hat{\mu} \pm \underline{12.7}\gamma$ for a Cauchy variable, in contrast with $\mu \pm \underline{1.96}\sigma$ required for Gaussian variables.

All statistical central moments of the Cauchy distribution are undefined, mean, variance, kurtosis and skewedness of the Cauchy distribution are undefined. The Cauchy distribution is considered an example of a “pathological” distribution function. Thus even when populations $\{L\}$ and $\{F\}$ are Gaussian, population $\{p\}$ [see Eqs. (17 – 19)] should be “pathologically” distributed and its mean and variance should be undefined. Sample values will be concentrated about $\hat{\mu}$, but the sample mean (\bar{x}) will be increasingly variable as the number observations increases, due to the increased probability of encountering sample points with a large absolute value (“outliers”). The distribution of the sample mean will be equal to the distribution of the outlying observations; i.e.,

Table 3: **Fitting Cauchy data generated with Eq. (33) setting $\gamma = 1/50$ and simplex optimization to the modified Hill equation. In all cases the optimization started with $y_0 = -10\%$, $y_m = 100\%$, $K_m = 0.1$ and $n = 2$; Δ_{init} was set as 0.1.**

r	θ_j	Simulated	Predicted	Range	Loops	Sk	Kr
3	y_0	-5	-5.86 (-12.41, -4.10)	(-26.71, 51.18)	3172	-2.44	11.0
	y_m	100	102.2 (59.3, 312.7)	($-1.7 \cdot 10^4$, $8.0 \cdot 10^5$)		3.25	13.6
	K_m	0.15	0.107 (0.042, 0.125)	(-0.101, 0.677)		2.443	77.5
	n	2	2.04 (1.98, 2.06)	(1.84, 2.61)		2.44	11.04
10	y_0	-5	-4.76 (-5.57, -4.04)	(-25.61, 108.07)	6100	4.91	31.8
	y_m	100	100.9 (94.5, 124.9)	($-3.6 \cdot 10^4$, $2.2 \cdot 10^5$)		4.81	26.7
	K_m	0.15	0.106 (0.098, 0.114)	(-0.102, 1.235)		4.919	31.8
	n	2	2.135 (2.127, 2.143)	(1.927, 3.264)		4.919	31.8
100	y_0	-5	-4.99 (-5.27, -4.71)	(-807, 549)	633	-4.376	170.9
	y_m	100	99.96 (98.05, 102.10)	($-1.2 \cdot 10^5$, $1.1 \cdot 10^5$)		1.774	125.7
	K_m	0.15	0.100 (0.097, 0.102)	(-7.925, 5.635)		-4.376	170
	n	2	2.017 (2.014, 2.019)	(-6.008, 7.552)		-4.376	170.9
2000	y_0	-5	-5.07 (-5.13, -5.01)	($-1.2 \cdot 10^4$, $3.0 \cdot 10^4$)	1051	-71.8	7112
	y_m	100	100.1 (99.70, 100.44)	($-1.2 \cdot 10^8$, $9.9 \cdot 10^6$)		-111	12841
	K_m	0.15	1.000 (0.099, 0.100)	(-118, 30.8)		-71.8	7112
	n	2	1.999 (1.998, 2.000)	(-115, 33)		-71.8	7111

The concentrations required by Eq. (24) were defined as: 0.001, 0.003, 0.01, 0.03, 0.1, 0.3 and 1; m is the number of $d_{i,j}$ values used to calculate medians, 95% confidence in terval and ranges. Parameters and heading have same meaning as used in Table 2; r indicates the number of random Cauchy values of type $f(U(0,1)_i | \gamma, 0) + y([D]_i | \{y_0, y_m, K_m, n\})$ [Eq. (33)] which were simulated for each concentration. Please notice that the units of K_m are irrelevant as long as they are equal to the units of $[D]$. See the text for further discussion.

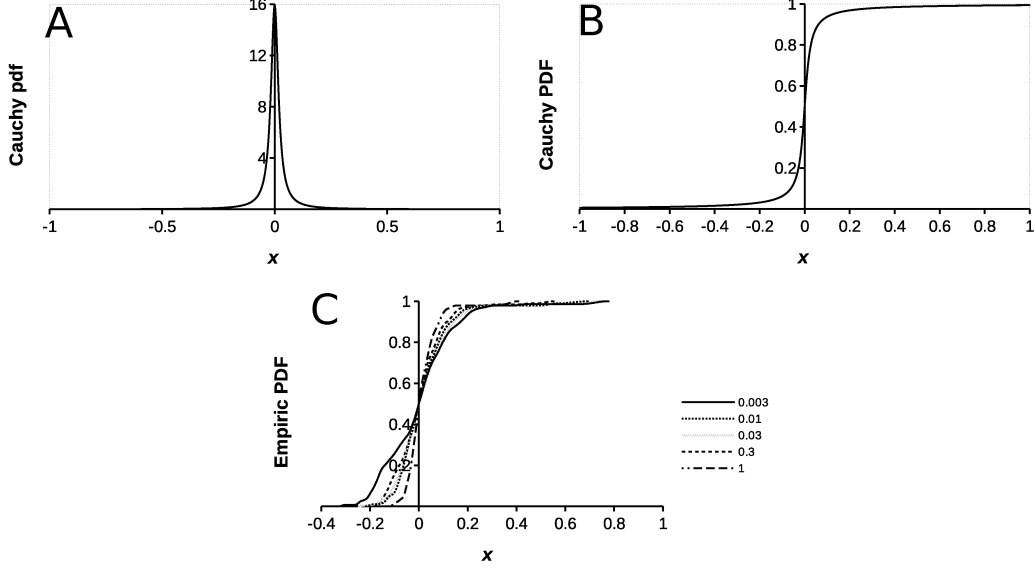


Figure 4: The Cauchy probability distribution and a set of representative empirical distribution functions for FIII from Quintana-Hernández [44] A- Cauchy probability density [Eq. (29)] function (pdf) calculated with $\gamma = 1/50$ and $\hat{\mu} = 0$. B- Cauchy probability distribution function (PDF) [Eq. (30)] calculated with $\gamma = 1/50$ and $\hat{\mu} = 0$. C- Several empirical probability distribution functions [28, 63] estimated for FIII at concentrations of 0.003, 0.01, 0.03 and 1 mg/ml. These curves were selected because they are representative of the ones obtained with other fractions. The empirical curves were plotted after subtracting the median of each killed cells fraction from the remaining values in the set. Other details in the text of the communication.

the sample mean is just an estimator of any single outlying observation from the sample. Similarly, calculating the sample variance will result in values which grow larger as more observations are considered [59–61].

Lemma 1. [Wilks [62], pg. 156] If x is a random variable having a PDF $F(x)$ then the random variable $y = F(x)$ has the rectangular distribution $R(\frac{1}{2}, 1)$.

Proof. This follows at once from the fact that the PDF of y is

$$G(y) = P[F(x) \leq y] = \begin{cases} 1, & y > 1 \\ y, & 0 < y \leq 1 \\ 0, & y \leq 0 \end{cases} \quad (31)$$

which is the pdf of the rectangular distribution $R(\frac{1}{2}, 1)$. \square

Wilks' [62] $R(\frac{1}{2}, 1)$, is denoted $U[0, 1]$ in this paper. Lemma 1 enables to simulate random variables distributed as $c(x \mid \{\gamma, \hat{\mu}\})$ using uniform random variables $U(0, 1)$ and the following expression

$$\Psi_C[U(0, 1)_i \mid \{\gamma, \hat{\mu}\}] = \hat{\mu} + \gamma \cdot \tan\left(\pi \cdot \left[U(0, 1)_i - \frac{1}{2}\right]\right). \quad (32)$$

Figure 4 presents a plot of a Cauchy probability density function (pdf) [Eq. (29)] calculated with $\gamma = 1/50$ and $\hat{\mu} = 0$ (Panel 4A), and a Cauchy probability distribution function (PDF) [Eq.

(30)] also calculated with $\gamma = 1/50$ and $\widehat{\mu} = 0$ (Panel 4B). Also in Figure 4 (Panel 4C) is a selection of empirical distribution functions [28, 63] determined for the sets of killed cells fractions observed with FIII [44]; this set was representative of other observed with the remaining fractions in Figures 2 and 3. Sets $\{L\}$ and $\{F\}$ [Eqs. (17) and (18)] were found not to be Gaussian using the Jarque-Bera [41] and Shapiro-Wilks [42] test, this only means that in addition to their most likely “pathological” distribution the precise nature of this distribution remains unknown. Yet, Figure 4C suggests that the empirical PDF of data in Figures 2 and 3 resemble the Cauchy PDF in Figure 4B.

To test the procedure discussed in this paper Cauchy-distributed data sets were generated using Monte Carlo simulation combining Eqs. (24) and (32) as

$$\begin{aligned} \Psi_{HC} \langle [D]_i \mid \{ \gamma, \widehat{\mu} = y([D]_i \mid \{y_0, y_m, K_m, n\}) \} \rangle_{i=1, \dots, m} = \dots \\ \dots = \left\{ y_0 + \frac{y_m}{1 + \left(\frac{K_m}{[D]_i} \right)^n} + \gamma \cdot \tan \left(\pi \cdot \left[U(0, 1)_i - \frac{1}{2} \right] \right) \right\}_{i=1, \dots, m} \end{aligned} \quad (33)$$

and used to calculate data sets, and processed as done with the data of Quintana-Hernández [44].

Some results of the fits of Eq. (24) to Cauchy data appear in Table 3 together with their apparent sample skewness [64, 65] calculated as

$$Sk = \frac{\frac{1}{m} \sum_{i=1}^m (x_i - \bar{x})^3}{\left[\frac{1}{m} \sum_{i=1}^m (x_i - \bar{x})^2 \right]^{3/2}} \quad (34)$$

and their apparent sample kurtosis calculated as

$$Kr = \frac{\frac{1}{m} \sum_{i=1}^m (x_i - \bar{x})^4}{\left[\frac{1}{m} \sum_{i=1}^m (x_i - \bar{x})^2 \right]^2} \quad (35)$$

where \bar{x} is the sample mean. The definition represented by Eq. (35) is presented here since there are controversies and discrepancies in the definition and interpretation of “kurtosis” and “excess kurtosis” or “Pearson’s kurtosis”, in the literature [65–75], kurtosis is used here in sense of Moors [73]:

“High kurtosis, therefore, may arise in two situations: (a) concentration of probability mass near μ (corresponding to a peaked unimodal distribution) and (b) concentration of probability mass in the tails of the distribution.”

In spite of their undefined central moments, both conditions occur in Cauchy-distributed variables if mean is replaced by median in the preceding Moors’ quote (see Figure 5). Estimated Sk and Kr were incompatible to the ones expected for Gaussian variables ($Sk = 0$, $Kr = 3$), this is not surprising since the data subject of the simplex optimization were generated for Cauchy-distributed random variables. The values of $Sk > 0$ indicate that the parameter estimates are asymmetrically distributed about the mean (median?), and Sk increases with sample size. Thus the parameter estimates are not exactly Cauchy-distributed either [27, 28]. Data in Tables 3 through 5 are very leptokurtic, clustered about the median, but extreme values are observed

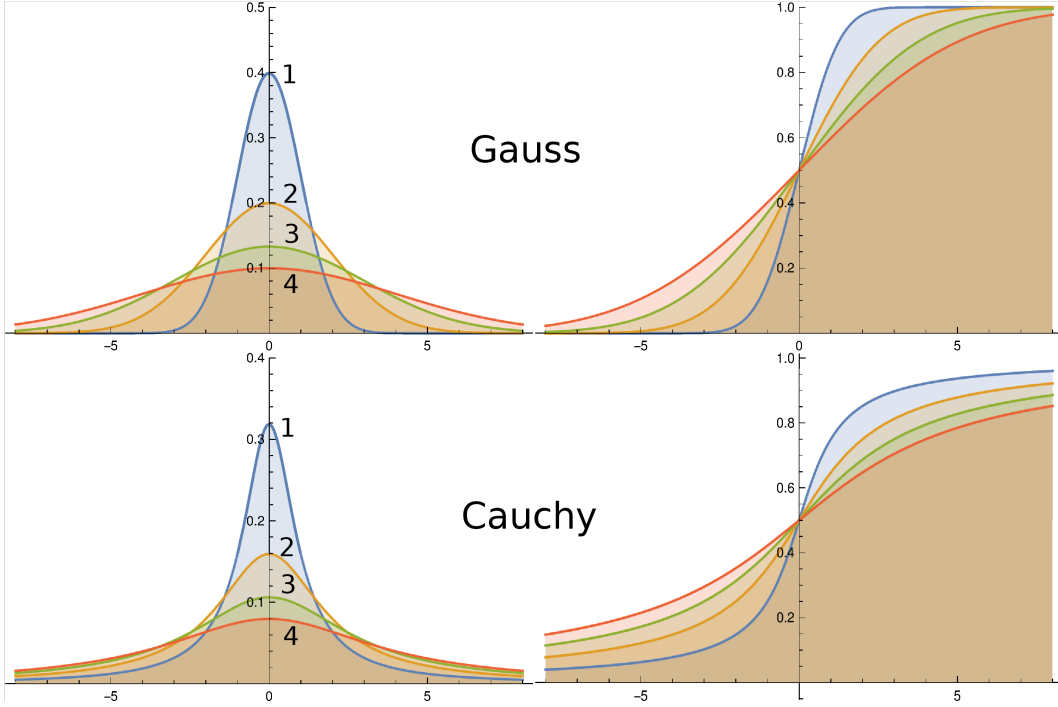


Figure 5: **Gauss and Cauchy probability density (pdf, left panels) and probability distribution (PDF, right panels) functions.** The functions are centered at the Gauss mean ($\mu = 0$) and the Cauchy median ($\hat{\mu} = 0$). Upper left: Gauss pdf; upper right: Gauss PDF; lower left: Cauchy pdf; lower right: Cauchy PDF. Numbers near the Gauss curves indicate the value of the variance ($\sigma^2 = 1, 2, 3$ or 4), numbers near the Cauchy curves indicate the value of the width factor ($\gamma = 1, 2, 3$ or 4). The figure enables a naked eye comparison of the two distributions, and shows that the Cauchy distribution has a sharper peak (most evident when $\gamma = 1$ in the figure) at the median ($\hat{\mu}$) of the distribution, and has broader shoulders (particularly evident in the Cauchy PDF plot) as $|x| \rightarrow \infty$, both factors explain apparently higher kurtosis (Kr) sample estimates. Other details in the text of the communication.

as indicated by the parameters' ranges [76]. Yet, in spite of the wide ranges, 95% confidence intervals are relatively narrow suggesting strong clustering of data around the median. It may seem startling that raising the initial n did not improve consistently the final estimate of n , and worsened the estimations of the other parameters too. Table 3 shows that the parameters $\{\theta_i\}_{sim} = \{y_0 = 5\%, y_m = 100\%, \mathbf{K}_m = \mathbf{0.15}, n = 2\}$ used to simulate data distributed as Cauchy are well predicted if a simplex optimization is used. At least if the simplex is initiated with a “reasonable” set of parameters ($\{\theta_i\}_{init} = \{y_0 = 10\%, y_m = 100\%, \mathbf{K}_m = \mathbf{0.1}, n = 2\}$).

Table 4 presents data generated with Eq. (33) using a parameter set $\{\theta\}_{sim} = \{y_0 = 5\%, y_m = 100\%, \mathbf{K}_m = \mathbf{0.01}, n = 15\}$, and the simplex optimization started from $\{\theta_i\}_{init} = \{y_0 = 10\%, y_m = 100\%, \mathbf{K}_m = \mathbf{0.1}, n = 2\}$ as in Table 3. As seen in the Table 4, y_0 , y_m , and K_m are well estimated using the simplex minimization described. Yet, $n \neq 15$ in all instances presented in Table 4.

To check if starting the simplex from higher values of n improves n estimate, in Table 5 presents data calculated for *exactly the same Monte Carlo data used in Table 4*, but starting the simplex optimization with $\{\theta_i\}_{init} = \{y_0 = 10\%, y_m = 100\%, \mathbf{K}_m = \mathbf{0.1}, n = 10\}$. As indicated by the discussion in Section B.1 and shown in Figure 6, raising the initial value of $n = 10$ did not improve the estimation of the parameter. More surprising was that **rising the initial value of**

n worsened the estimates of all the other parameters characterizing Eq. (24). Taken together the results in tables 4 and 5, suggests that n is the most difficult parameter to estimate in Equation (24). The difficulty to estimate n correctly agrees with the discussion on $\omega(n)$ done in Section B.1.

It is necessary to point out several features, some very evident and others not so much, of data in Tables 3 – 5. In the three tables, specially in optimizations with larger r , some sets of Monte Carlo simulated data did not reach Condition 2, and the optimization stopped according to Condition 3 (numbers with asterisks). One instance of this situation appears in each Table 3 – 5, but each of these data sets could have been replaced by results obtained for other sets of pseudorandom data generated under similar conditions where Condition 2 was indeed achieved, i.e., failure to comply with Condition 2 did not always occurred. The instances where Condition 3 stopped calculations were included in the tables to show that they do occur. Another feature apparent in Tables 3 – 5 is that although all set of parameters are leptokurtic and skewed, Kr increased with the number of points (r) used for each concentration in the optimization, Sk did not increase as much as Kr but was noticeably large with $r = 2000$. Sk and Kr depend on the 2nd, 3rd and 4th central moments of a distribution which do not exist for the Cauchy distribution, thus sample values cannot converge towards any population value as required by sampling theory [62], since population mean, variance, skewness and kurtosis do not exist for Cauchy distributed data. Sample variance, for example, grows with sample size. Since the probability density function of the Cauchy distribution has long tails, the odds for large values to occur are not negligible. This makes the mean jump considerably even when several hundred or thousand random numbers are averaged [59–61]. Yet, with all the uncertainties, the Sk and Kr estimates clearly indicate that data in tables 3 – 5 are non-Gaussian.

3.2.2. Fitting Gauss distributed data to the modified Hill equation.

To evaluate the behavior of Eq. (24) when Gaussian variables are adjusted to the equation, normal variates $N(u_i, s^2)$ generated as

$$\begin{aligned} \Psi_{HG} \left\{ [D]_i \mid \left[\sigma^2 = \varsigma, \mu = y \left([D]_i \mid \{y_0, y_m, K_m, n\} \right) \right] \right\}_{i=1, \dots, m} = \dots \\ \dots = \left\{ y_0 + \frac{y_m}{1 + (K_m/[D]_i)^n} + \varsigma \cdot N(0, 1)_i \right\}_{i=1, \dots, m}, \end{aligned} \quad (36)$$

was used to test the ability of the method proposed here to determine the parameters, with $\varsigma = \frac{s^2[y(x_i)]}{\bar{y}(x_i)}$, in which $s^2[y(x_i)]$ and $\bar{y}(x_i)$ were the simulated effects variances and means, respectively. Tables 6 to 8 follow the same sequence of changes of simulating sets $\{\theta_i\}_{sim}$ and initial values $\{\theta_i\}_{init}$ as Tables 3 to 5, but data adjusted to Eq. (24) was Gaussian and generated as indicated in the prior paragraph. As in the case of Cauchy distributed data in Section 3.2.1, y_0 , y_m , and K_m are well estimated using the simplex minimization described. Yet, $n \neq 15$ (\neq symbol is used to mean very significantly different) in all instances presented in Table 4, this suggests that n is the most difficult parameter to estimate if the initiating value of n in the simplex is very different from the value used in the Monte Carlo simulation.

$\Delta_{init} = 0.1$ (used as initiation value in Tables 3 to 8) means that the initial parameters begin increasing by 10%. In calculations, not published here, the simulations in Tables 3 to 8 were carried out setting $\Delta_{init} = 0.5$, and yet $n \neq 15$, and the estimates of the other parameters became worse.

Table 4: **Fitting Cauchy data generated with Eq. (33) setting $\gamma = 1/50$ and simplex optimization to the modified Hill equation. In all cases the optimization started with $y_0 = -10\%$, $y_m = 100\%$, $K_m = 0.1$ and $n = 2$; Δ_{init} was set as 0.1.**

r	θ_j	Simulated	Predicted	Range	Loops	Sk	Kr
3	y_0^\bullet	-5	8.5 (-5.5, 41.0)	(-182.5, 95.9)	41029	1.260	3.145
	y_m	100	93.9 (-10 ²¹ , 7 · 10 ⁵)	(-9 · 10 ²² , 7 · 10 ¹¹)		-4.092	18.1
	K_m^\bullet	0.01	0.20 (0.06, 0.53)	(-0.07, 1.08)		1.260	3.145
	n^\bullet	15	11.8 (11.7, 12.2)	(11.6, 12.7)		1.026	5.352
10	y_0	-5	2.4 (1.2, 4.1)	(-358, 621)	2176	-4.995	30.0
	y_m	100	97.3 (-34.6, 100.0)	(-6 · 10 ⁴⁰ , 8 · 10 ⁴⁰)		2.065	25.7
	K_m	0.01	0.05 (0.02, 0.05)	(-3.57, 0.63)		-4.995	30.0
	n	15	28.55 (28.54, 28.56)	(24.9, 29.1)		4.995	30.0
100	y_0	-5	-5.9 (-6.2, -5.6)	(-19.3, 9.7)	26297	-12.2	255.4
	y_m	100	102.6(101.9, 103.7)	(-10 ¹³ , 10 ¹³)		25.6	670.7
	K_m	0.01	0.013 (0.010, 0.016)	(-0.3, 0.2)		-12.2	255.4
	n	15	11.196 (11.192, 11.199)	(-8.0, 21.0)		-12.2	255.4
2000	y_0	-5	26.5 (26.2, 26.8)	(-1.9 · 10 ⁴ , 10 ⁵)	932	106.3	12272
	y_m	100	59.3 (28.4, 63.6)	(-2 · 10 ⁶¹ , 2 · 10 ⁶⁰)		-113.6	13261.4
	K_m	0.01	0.063 (0.060, 0.065)	(-197.2, 1105.3)		106.3	12272
	n	15	31.9 (31.9, 31.9)	(-165.4, 1137.1)		106.3	12272

Parameters and heading have same meaning as used in Table 2; r indicates the number of random Cauchy values fitted to Eq. (24) which were exactly the same used in Table 3. Please notice that the units of K_m are irrelevant as long as they are equal to the units of [D]. Parameter names (θ_i) with a bullet (\bullet) indicated that, tested with the Jarque-Bera test, the probability that the parameter is not Gaussian by chance is not too low ($P = 0.03$). Number of loops with an asterisk indicates the optimization stopped after fulfilling Condition 3. Other conditions as in Table 3. Please notice that $n \neq 15$ in all instances. See the text of the communication for further discussion.

This agrees with the discussion about Eqs. (40) to (43) in Section B.1 which holds for Gaussian random variables, since the discussion in Section B.1 is distribution independent.

3.3. The Boltzmann probability distribution function.

A function commonly used to describe data from diverse empirical sources is the Boltzmann *probability distribution function* (*pdf*), one of its forms is Eq. (48), revised in [77]. Boltzmann function first partial derivatives, for a form commonly used in electrophysiology [77, 78], are Eqs. (49) and (50). In addition to the properties of the Boltzmann function considered in [77], more details on this distribution are presented in Section C and Figure 7.

3.3.1. Using the Boltzmann distribution function to fit Gaussian data

To evaluate the behavior of Eq. (48) Gaussian variables are adjusted to the equation, normal variates $N(u_i, s^2)$ generated as

$$\Psi_{BG} \left(V_i \mid \left\{ \varsigma = \sigma^2, y(V_i \mid \{V_{\frac{1}{2}}, \kappa\}) \right\}_{i=1, \dots, m} \right) = \left\{ \frac{1}{1 + \exp\left(-\frac{V_i - V_{\frac{1}{2}}}{k}\right)} + \varsigma N(0, 1)_i \right\}_{i=1, \dots, m} \quad (37)$$

setting $\varsigma = \frac{s^2[y(x_i)]}{y(x_i)}$, where $s^2[y(x_i)]$ and $\overline{y(x_i)}$ are sample variance and mean, respectively, of the simulated effects. Results are shown in Tables 9 and 10.

Tables 9 and 10 shows considerable independence between initial and predicted $\{\theta_j\}$ and r values, since in all cases the optimization produced remarkably similar estimates of $V_{\frac{1}{2}}$ and κ in agreement with the discussion of Eqs. (49) and (50). Optimizations presented in Tables 9 and 10 was started with $\Delta_{init} = 0.5$, and was even better when $\Delta_{init} = 0.1$. With $\Delta_{init} = 0.1$, it made no relevant difference for predicting the parameters used to simulate $\{V_{\frac{1}{2}}, \kappa\} = \{-40, 10\}$ to start optimization with $\{\theta_i\}_{init} = \{V_{\frac{1}{2}}, \kappa\}_{init}$ set as : $\{-20, 1\}$, $\{-20, 5\}$, $\{-20, 20\}$ or $\{-60, 20\}$. With $\Delta_{init} = 0.1$, it was to any practical purpose irrelevant, if the number of replicates (r) was: 3, 10, 100 or 2000. Tables 9 and 10 show that parameters are also leptokurtic and not Gaussian (as shown by Jarque-Bera and Shapiro-Wilks tests), but with low Sk , and that Sk and Kr seem largely independent of sample sizes (r) and $\{\theta_j\}_{init}$. Ranges of predicted parameters in Tables 9 and 10 were quite narrow, the Boltzmann function [Eq. (48)] seems easier to optimize to the correct parameters values that the Hill equation [Eq. (24)].

3.3.2. Using the Boltzmann distribution function to fit Cauchy data

The most common use of the Boltzmann function in electrophysiology is to fit normalized ionic currents [77–79]. To do this, ionic currents are measured at a broad range of membrane potentials, and the currents recorded are divided by the maximum value observed at the most negative potentials tested, in the case of sodium current in excitable cells. Normalized currents (or any other parameter) which results from random variable quotients are likely to obey a Cauchy resembling distribution.

Table 11 present data calculated as in Table 10 except for the data fit to the Boltzmann equation

Table 5: **Fitting Cauchy data generated with Eq. (33) setting $\gamma = 1/50$ and simplex optimization to the modified Hill equation. In all cases the optimization started with $y_0 = -10\%$, $y_m = 100\%$, $K_m = 0.1$ and $n = 10$; Δ_{init} was set as 0.1.**

r	θ_j	Simulated	Predicted	Range	Loops	Sk	Kr
3	y_0	-5	8.64 (-5.45, 41.02)	(-18.1, 95.9)	31829	1.260	3.147
	y_m	100	93.7 (-1.6 · 10 ²¹ , 1.8 · 10 ⁶)	(-10 ²² , 2.2 · 10 ¹¹)		-4.072	18.0
	K_m	0.01	0.20 (0.06, 0.52)	(-0.07, 1.07)		1.260	3.147
	n	15	11.84 (11.70, 12.17)	(11.6, 12.72)		1.260	3.147
10	y_0	-5	2.38 (1.22, 4.05)	(-357.8, 62.1)	2176	-4.995	30.0
	y_m	100	84.6 (-3.0 · 10 ⁵ , 92.0)	(-10 ¹¹ , 4 · 10 ⁷)		-4.89	30.79
	K_m	0.01	-0.007 (-0.023, 0.007)	(-0.334, 0.363)		-0.352	8.142
	n	15	9.46 (9.45, 9.48)	(9.3, 9.8)		-0.352	8.142
100	y_0	-5	-4.19 (-4.50, -3.88)	(-1925.1, 972.1)	1060	-12.2	255.4
	y_m	100	97.61 (96.66, 98.39)	(-9 · 10 ¹⁶ , 10 ¹⁸)		25.6	669.7
	K_m	0.01	0.006 (0.003, 0.009)	(-19.2, 9.8)		-12.2	255.4
	n	15	14.99 (14.99, 15.00)	(-4.2, 24.8)		106.3	255.4
2000	y_0	-5	26.5 (26.2, 26.8)	(-1.9 · 10 ⁴ , 10 ⁵)	2010	32.9	12272.1
	y_m	100	59.3 (28.4, 63.6)	(-3 · 10 ⁶¹ , 3 · 10 ⁶¹)		-113.6	13261.5
	K_m	0.01	0.07 (0.06, 0.07)	(-197.2, 1105.3)		106.3	12272.1
	n	15	31.98 (31.97, 31.98)	(-165.2, 1137.2)		106.3	12272.1

Table 5 presents results calculated for *exactly the same* Monte Carlo data used in Table 4, but starting the simplex optimization with $\{y_0 = 10\%, y_m = 100\%, K_m = 0.1, n = 10\}$. Parameters and heading have same meaning as used in Table 2; r indicates the number of random Cauchy values calculated with Eq. (33) were simulated for each concentration. Please notice that the units of K_m are irrelevant as long as they are equal to the units of [D]. Other conditions as in Table 3. Please notice that $n \neq 15$ in all instances. See the text of the communication for further discussion.

Table 6: **Fitting Gauss data (Ψ_{HG}) generated with Eq. (36) setting $\varsigma = 0.05$ and simplex optimization to the modified Hill equation. In all cases the optimization started with $y_0 = -10\%$, $y_m = 100\%$, $K_m = 0.1$ and $n = 2$; Δ_{init} was set as 0.1.**

r	θ_j	Simulated	Predicted	Range	Loops	Sk	Kr
3	y_0^*	-5	-3.68 (-6.44, -10.16)	(-14.03, 9.22)	230969	0.314	2.944
	y_m	100	82.8 (-937.4, 71.8)	$(-4 \cdot 10^7, 2 \cdot 10^7)$		-1.864	11.1
	K_m^*	0.15	0.12 (0.09, 0.15)	(0.02, 0.25)		0.314	2.944
	n^*	2	3.20 (3.17, 3.22)	(3.1, 3.3)		0.314	2.944
10	y_0^*	-5	-4.09 (-5.48, -2.68)	(-152.2, 7.5)	6253	-0.167	2.277
	y_m	100	101.7 (65.2, 141.1)	$(-10^5, 1.7 \cdot 10^5)$		0.946	11.7
	K_m^*	0.15	0.15 (0.14, 0.16)	(0.04, 0.27)		-0.167	2.277
	n^*	2	1.91 (1.90, 1.93)	(1.8, 2.0)		-0.167	2.277
100	y_0^*	-5	-4.96 (-5.33, -4.58)	(-20.3, 9.7)	745	-0.069	2.912
	y_m	100	97.5 (94.0, 100.9)	$(-6 \cdot 10^5, 5 \cdot 10^5)$		-0.081	21.6
	K_m^*	0.15	0.143 (0.139, 0.146)	(-0.01, 0.29)		-0.069	2.912
	n^*	2	2.121 (2.117, 2.124)	(2.0, 2.3)		-0.069	2.912
2000	y_0^*	-5	-5.18 (-5.27, -5.09)	(-5.3 -5.1)	1024002*	0.032	2.951
	y_m	100	101.9 (101.2, 102.7)	$(-3 \cdot 10^5, 4 \cdot 10^5)$		0.250	20.1
	K_m^*	0.15	0.152 (0.151, 0.152)	(-0.05, 0.34)		0.032	2.951
	n^*	2	2.013 (2.012, 2.014)	(1.8, 2.2)		0.032	2.951

Parameters and heading have same meaning as used in Table 2; r indicates the number of random Gaussian values of type $N(\mu, 0.05 \cdot \mu)$ with $\mu = y([D] \mid \{y_0, y_m, K_m, n\})$ which were simulated for each concentration. Parameter names (θ_j) with an asterisk indicated that Gaussianity cannot be ruled out when Jarque-Bera test is used ($0.95 > P > 0.05$), for all y_m 's $P < 10^{-6}$ using the same test. Number of loops with an asterisk indicates the optimization stopped after fulfilling Condition 3. Other conditions as in Table 3, see the text of the communication for further discussion.

Table 7: **Fitting Gauss data (Ψ_{HG}) generated with Eq. (36) setting $\varsigma = 0.05$ and simplex optimization to the modified Hill equation. In all cases the optimization started with $y_0 = -10\%$, $y_m = 100\%$, $K_m = 0.1$ and $n = 2$; Δ_{init} was set as 0.1.**

r	θ_j	Simulated	Predicted	Range	Loops	Sk	Kr
3	y_0^*	-5	-9.3 (-10.9, -5.6)	(-19.9, 3.6)	70873	0.420	2.941
	y_m	100	109.2 (104.1, 115.9)	(-902.9, 4401.8)		3.693	16.4
	K_m^*	0.01	0.02 (0.00, 0.05)	(-0.09, 0.14)		0.420	2.941
	n^*	15	2.55 (2.54, 2.59)	(2.5, 2.7)		0.420	2.941
10	y_0^*	-5	-6.40 (-7.72, -5.16)	(-14.2, -0.11)	17486	-0.381	2.843
	y_m	100	101.6 (98.7, 104.2)	($5 \cdot 10^4$, $5 \cdot 10^4$)		1.089	14.2
	K_m^*	0.01	0.005 (-0.008, 0.01747)	(-0.13, 0.11)		-0.381	2.843
	n^*	15	3.71 (3.69, 3.72)	(3.57, 3.81)		-0.381	2.843
100	y_0^*	-5	-6.32 (-6.71, -5.95)	(-20.9, 10.3)	31287	0.037	2.950
	y_m	100	101.4 (100.5, 102.3)	($-4 \cdot 10^5$, $4 \cdot 10^5$)		0.997	18.0
	K_m^*	0.01	0.010 (0.006, 0.013)	(-0.14, 0.18)		0.037	2.950
	n^*	15	4.604 (4.601, 4.608)	(4.5, 4.8)		0.037	2.950
2000	y_0^\bullet	-5	2.97 (-5.46, 11.43)	($-2 \cdot 10^3$, $2 \cdot 10^3$)	11061	0.046	3.019
	y_m	100	92.3 (71.6, 113.0)	($-2 \cdot 10^6$, $2 \cdot 10^6$)		0.028	20.8
	K_m^\bullet	0.01	-0.013 (-9.78, 7.11)	(-19.5, 19.8)		0.046	3.019
	n^\bullet	15	2.8 (2.7, 2.9)	(-16.8, 22.5)		0.046	3.019

Parameter names (θ_i) with an astreisk indicated that Gaussianity cannot be ruled out when Jarque-Bera test is used ($0.95 > P > 0.05$), for all y_m 's $P \ll 10^{-6}$ using the same test. Parameter names with a bullet (\bullet) indicate weak not Gaussianity ($P = 0.037$, Jarque-Bera test). Number of loops with an asterisk indicates the optimization stopped after fulfilling Condition 3. Other conditions as in Table 3. Please notice that $n \neq 15$ in all instances. See the text of the communication for further discussion.

Table 8: **Fitting Gauss data (Ψ_{HG}) generated with Eq. (36) setting $\varsigma = 0.05$ and simplex optimization to the modified Hill equation. In all cases the optimization started with $y_0 = -10\%$, $y_m = 100\%$, $K_m = 0.1$ and $n = 10$.**

r	θ_j	Simulated	Predicted	Range	Loops	Sk	Kr
3	y_0^\bullet	-5	1.50 (-1.06, 1.67)	(-11.0, 50.8)	38091	1.716	4.595
	y_m	100	93.74 ($-1.7 \cdot 10^{19}$, $1.8 \cdot 10^6$)	(10^{23} , $2 \cdot 10^{11}$)		-4.072	18.0
	K_m^\bullet	0.01	0.20 (0.06, 0.52)	(-0.06, 1.07)		1.260	3.147
	n^\bullet	15	1.42 (1.40, 1.48)	(1.4, 1.6)		0.704	2.905
10	y_0	-5	0.46 (-1.40, 3.04)	(-9.8, 53.0)	8577	1.751	4.582
	y_m	100	94.5 ($-6 \cdot 10^{12}$, 98.8)	($-4 \cdot 10^{23}$, $5 \cdot 10^{15}$)		-2.854	9.716
	K_m	0.01	0.03 (0.01, 0.06)	(-0.07, 0.56)		1.751	4.582
	n	15	16.6 (16.5, 16.6)	(16.5, 17.1)		1.751	4.582
100	y_0	-5	15.0 (12.4, 18.9)	(-19.7, 108.4)	1262	1.264	3.355
	y_m	100	78.9 ($-3 \cdot 10^{78}$, 82.4)	($-3 \cdot 10^{107}$, 10^{48})		-2.558	8.519
	K_m	0.01	0.10 (0.08, 0.14)	(-0.2, 1)		1.264	3.355
	n	15	60.1 (60.1, 60.2)	(60, 61)		1.264	3.355
2000	y_0	-5	19.2 (18.8, 19.6)	(-22.5, 112.7)	3226	1.140	3.261
	y_m	100	72.7 (68.9, 74.0)	($-4 \cdot 10^{84}$, $5 \cdot 10^{39}$)		-2.280	6.609
	K_m	0.01	0.094 (0.091, 0.098)	(-0.32, 1.03)		1.140	3.261
	n	15	45.1 (45.0, 45.1)	(44.6, 46.0)		1.140	3.261

Table 8 presents data calculated for *exactly the same* Monte Carlo data used in Table 7, but starting the simplex optimization with $\{y_0 = 10\%, y_m = 100\%, K_m = 0.1, n = 10\}$. and heading have same meaning as used in Table 2; r indicates the number of random Gaussian values of type $N(\mu, \sigma^2 = 0.05 \cdot \mu)$ with $\mu = y(x_i | \{V_{\frac{1}{2}}, \kappa_j\}) = \frac{1}{1+e^{-(x_i-V_{\frac{1}{2}})/\kappa}}$ which were simulated for each concentration. Parameter names (θ_j) with an bullet (\bullet) indicated that the propability of Gaussianity when Jarque-Bera test is used is $P \approx 9 \cdot 10^{-4}$, for all parameters without a bullet $P \ll 10^{-6}$ using the same test. Please notice that $n \neq 15$ in all instances. See the text for further discussion.

Table 9: **Fitting Gaussian data generated Eq. (37) to the Boltzmann equation with the simplex optimization. In all cases the optimization started with $V_{\frac{1}{2}} = -20$, $\kappa = 1$ and $\Delta_{\text{init}} = 0.5$.**

r	θ_j	Simulated	Predicted	Range	Loops	Sk	Kr
3	$V_{\frac{1}{2}}$	-40	-41.531 (-41.536, -41.530)	(-41.556, -41.530)	1766	-1.899	5.483
	κ	10	9.403 (9.401, 9.404)	(9.38, 9.43)		0.331	4.555
10	$V_{\frac{1}{2}}$	-40	-40.0585 (-40.062, -40.058)	(-40.08, -40.06)	478	-1.799	5.128
	κ	10	9.9416 (9.9415, 9.9417)	(9.92, 9.96)		0.019	4.478
100	$V_{\frac{1}{2}}$	-40	-39.922 (-39.925, -39.921)	(-39.95, -39.93)	381	-1.779	5.055
	κ	10	10.0322 (10.0322, 10.0323)	(10.01, 10.05)		-0.004	4.441
2000	$V_{\frac{1}{2}}$	-40	-39.991 (-39.991, -39.990)	(-40.014, -39.989)	242	-1.785	5.078
	κ	10	10.005 (10.005, 10.005)	(9.98, 10.03)		0.007	4.453

The V values required by Eq. (48) were defined as: -100, -80, -60, -40, -20, 0, 20, 40, 50, 80 and 100; m is the number of $d_{j,i}$ values used to calculate medians, 95% confidence interval and ranges. Table heading have same meaning as used in Table 2; r indicates the number of random Gaussian values of type $N(\mu, \sigma^2 = 0.05 \cdot \mu)$ with $\mu = y(x_i \mid \{V_{\frac{1}{2}}, \kappa\}) = \frac{1}{1 + e^{-(x_i - V_{\frac{1}{2}})/\kappa}}$ which were simulated for each concentration. See the text for further discussion.

Table 10: Fitting Gaussian data generated Eq. (37) to the Boltzmann equation with the simplex optimization. In all cases the optimization started with $V_{\frac{1}{2}} = -60$, $\kappa = 20$ and $\Delta_{\text{init}} = 0.5$.

r	θ_j	Simulated	Predicted	Range	Loops	Sk	Kr
3	$V_{\frac{1}{2}}$	-40	-38.493 (-38.498, -38.492)	(-38.52, -38.49)	1024003*	-1.654	4.567
	κ	10	10.591 (10.590, 10.593)	(10.57, 10.61)		-0.181	4.104
10	$V_{\frac{1}{2}}$	-40	-39.927 (-39.931, -39.927)	(-39.950, -39.926)	1768	-1.768	5.014
	κ	10	9.9416 (9.9415, 9.9417)	(9.92, 9.96)		-0.004	4.420
100	$V_{\frac{1}{2}}$	-40	-40.163 (-40.166, -40.162)	(-40.19, -40.16)	340	-1.798	5.127
	κ	10	9.942 (9.942, 9.942)	(9.92, 9.96)		0.038	4.477
2000	$V_{\frac{1}{2}}$	-40	-40.005 (-40.005, -40.004)	(-40.028, -40.003)	327	-1.786	5.080
	κ	10	10.002 (10.003, 10.002)	(9.98, 10.02)		0.010	4.454

Table heading have same meaning as used in Table 2; r indicates the number of random Gaussian values of type $N(\mu, \sigma^2 = 0.05 \cdot \mu)$ with $\mu = y(x_i | \{V_{\frac{1}{2}}, \kappa\}) = \frac{1}{1 + e^{-(x_i - V_{\frac{1}{2}})/\kappa}}$ which were simulated for each concentration. See the text for further discussion. Number of loops with an asterisk indicates the the optimization stoped after fulfilling Condition 3. Other details as in Table 9

Table 11: **Fitting Gaussian data generated Eq. (37) to the Boltzmann equation with the simplex optimization. In all cases the optimization started with $V_{\frac{1}{2}} = -60$, $\kappa = 20$ and $\Delta_{\text{init}} = 0.5$.**

r	θ_j	Simulated	Predicted	Range	Loops	Sk	Kr
3	$V_{\frac{1}{2}}$	-40	-40.395 (-40.399, -40.394)	(-40.419, -40.394)	210	-1.866	5.381
	κ	10	9.631 (9.630, 9.632)	(9.610, 9.643)		-0.181	4.104
10	$V_{\frac{1}{2}}$	-40	-39.985 (-39.989, -39.984)	(-40.007, -39.983)	508	-1.676	4.672
	κ	10	10.5380 (10.5378, 10.5380)	(10.5176, 10.5584)		0.011	4.232
100	$V_{\frac{1}{2}}$	-40	-40.055 (-40.058, -40.054)	(-40.079, -40.053)	317	-1.777	5.045
	κ	10	10.0451 (10.0451, 10.0452)	(10.024, 10.066)		0.017	4.437
2000	$V_{\frac{1}{2}}$	-40	-39.978 (-39.978, -39.978)	(-40.00, -39.98)	635	-1.790	5.094
	κ	10	9.9841 (9.9841, 9.9841)	(9.96, 10.01)		0.005	4.461

Table heading have same meaning as used in Table 2; r indicates the number of random Gaussian values of type $N(\mu, \sigma^2 = 0.05 \cdot \mu)$ with $\mu = y(x_i | \{V_{\frac{1}{2}}, \kappa\}) = \frac{1}{1 + e^{-\frac{(x_i - V_{\frac{1}{2}})}{\kappa}}}$ which were simulated for each concentration. See the text for further discussion. Other details as in Table 9.

wich was distributed a Cauchy, generated as

$$\Psi_{BC} \langle V_i | [\gamma, y(V_i | \{V_{\frac{1}{2}}, \kappa\})] \rangle_{i=1, \dots, m} = \dots$$

$$\dots = \left\{ \frac{1}{1 + \exp\left(-\frac{V_i - V_{\frac{1}{2}}}{\kappa}\right)} + \gamma \cdot \tan\left(\pi \cdot \left[U(0, 1)_i - \frac{1}{2}\right] + 1\right) \right\}_{i=1, \dots, m}, \quad (38)$$

$\gamma = \frac{2}{50}$ for all data in Table 11. Comparing Tables 10 and 11 may be appreciated that data predicted did not differ much whether the input is Gaussian or Cauchyan when fitted to the Boltzmann equation. As it was the case with Gaussian data, the fit with Cauchyan data was faster and better using $\Delta_{\text{init}} = 0.5$. In all cases sample $Kr > 3$ and sample $Sk < 0$ for predicted $V_{\frac{1}{2}}$. Jarque-Bera and Shapiro-Wilks tests indicated that predicted parameters were not Gaussian ($P < 10^{-6}$).

4. Concluding remarks.

Estimating the uncertainty of objective function parameters which are not linearly independent is a challenging problem of regression analysis [2, 3]. Iterative processes used in nonlinear

optimization need a starting set of parameters $\{\theta\}_{init}$ which, if close enough to the global maximum or minimum, enables the algorithm to render $\{\theta\}_{opt}$, the best possible set of parameters and to minimize residual differences between empirical points and the objective function. Part of the difficulty is the existence of local minima or maxima towards which the iterative optimization processes (such as the simplex algorithm [39]) may converge, failing to reach the global minimum or maximum. At any of these local minima or maxima the objective function gradient respect to the independent variable(s) becomes null [See Eq. (1)].

Estimating parameter uncertainties in linear regression analysis may be simpler, and is usually done by least squares analysis (also called ℓ_2 -norm) which minimizes the sum of residuals squares and produces a set of simultaneous linearly independent equations, which may be solved to determine regression parameters. The least squares procedure has the pitfall of giving undue weight to outliers. The undue weight of outliers may be prevented by minimizing the sum of absolute values of residuals (also called ℓ_1 -norm) but it has no analytical solution for neither parameter nor parameter uncertainty determination [80, 81].

In many real word situations the fluctuating nature of the *obf* makes lots of sense. Hill and Boltzmann equations are both used to describe interactions between particles or molecules, the structures of those molecules and their interactions fluctuate at any temperature distinct from 0°K [54, 55, 77]. At the subatomic level, quantum physics is totally based on random processes [82]. Neurotransmitter release is a Poissonian process [83] and cell physiology is critically dependent on random cell membrane ionic permeability changes [16]. As indicated by this small and arbitrary selection of physical realities indicates, demanding that the *obf* is static and reality fluctuates randomly about it, is only an arbitrary choice.

Even at global optimum of a regression, residual differences between the objective function and empirical data remain. Here it is proposed that residuals may be seen as a measure of uncertainty of an objective function to describe a set of empirical data. That is, empirical data are taken as variables produced by the *obf* which fluctuates randomly describing fuzzily the relation between dependent and independent variables. Fluctuations remain no matter if we know the objective function's parameters at the global optimum.

Uncertainties associated with the parameters at the optimum $\{\{\theta_{j=1,\dots,k}\}_{opt}, \text{Eq. (1)}\}$ named here $\{\vartheta_{j,i}\}_{\substack{j=1,2,\dots,k \\ i=1,2,\dots,m}}$, are defined by Eq. (10). These sets are values of the objective function parameter θ_j calculated by adding or subtracting each of m residuals from the objective function. It is proposed here that $\{\vartheta_{j,i}\}_{\substack{j=1,2,\dots,k \\ i=1,2,\dots,m}}$ sets may be used to estimate the uncertainty of each element of the $\{\theta_j\}$ sets. Our results suggest that this may be done using nonparametric statistics even in cases (such as the Cauchy distribution [27–29]) where central moments are undefined.

Sets of empirical variables [44] and two functions widely used to describe data in science, the Boltzmann [30, 31] and the Hill functions [54, 55] are used here to evaluate the *first derivative at the optimum* analysis (*fdao*) usefulness. The Boltzmann function was used in a form common in electrophysiology [Eq. (48)] [77, 78, 84] and Hill function [Eq. (24)] modified to include shift in the baseline often occurring in experimental situations. The first derivatives of those functions and the analysis at the optimum properties (Sections B.1 and C.1.

In Section 3.1 empirical data shown in Figures 2 and 3, as well as Tables 1 and 2 present median values (•) and 95% confidence intervals (CI, bars) of anti-neoplastic effects produced by compounds isolated from *P. constellatum* (Savigny, 1816), a marine animal [44]. As seen in Figure

2, 95% CI are very asymmetric and broad suggesting negative outliers.

When data in Fig. 2 was plotted as in Fig. 3, clipping the lower axis at -20%, a sigmoid resemblance of the median data at the different concentrations became evident. Lines in Fig. 3 were drawn using Eq. (24) fitted using simplex optimization (described in Sections 2.2.1 and 3.1), are close to the median determined at each concentration. The parameters used are in Table 1, and some additional sample statistical properties are in Table 2. As it would be expected if the data would be Cauchy- or Cauchy-like-distributed, parameter ranges fluctuate between wide and huge, data appear to be strongly skewed and very leptokurtic. In case of fraction FIV the simplex stopped on Condition 3 since Condition 2 could not be achieved in ≈ 3 h, but in the other cases Condition 2 was reached with ≤ 21432 algorithm iterations in few minutes. Perhaps the most interesting feature of the parameters describing the curves in Table 1 is that the 95% CIs are narrow in spite of the parameter ranges, this can indeed be expected if the parameters are strongly leptokurtic and mostly packed around the medians as it is the case for the Cauchy distribution.

Figure 4 presents Cauchy probability density [Eq. (29)] function (pdf) and the Cauchy PDF [Eq. (30)] calculated with $\gamma = 1/50$ and $\hat{\mu} = 0$. The figure also depicts several empirical probability distribution [28, 63] curves estimated for FIII at diverse concentrations. This curves were selected because are representative of the ones obtained with other fractions. Comparing panels 4B and 4C in the figure, it is apparent that there is a good agreement between the empirical PDF and the Cauchy PDF. To check how does the ve analysis performs when applied to Cauchy data, Cauchyan [D] values were generated as explained in Section 3.2.1 and used as input to Eq. (24) using variable θ_j and Δ_{init} starting increments for the simplex algorithm, the results are summarized in Tables 3 to 5. The empirical data [44] and parameters determined imputing Cauchy variables to the Hill equation [Eq. (24)] have several characteristics in common. Parameter ranges are broad, and extremely so in some cases, the parameters are apparently skewed and leptokurtic but the median parameter 95% CI are relatively narrow. In some cases the optimization stopped on Condition 3, the parameters calculated when this happened seemed “reasonable” since they did not look too different from the parameters obtained when the optimization ended on Condition 2. Although it was not extensively studied here, no $\{\theta\}$ or Δ_{init} values prone to produce endings with Condition 3 were identified. It is the author’s impression that ending on Condition 3 was more likely with larger sample sizes, and when samples were per chance more disperse and thus harder to optimize.

Optimizations using Cauchy data summarized in Tables 3 to 5 were all initiated with the same $\Delta_{init} = 0.1$ but different $\{\theta\}_{init}$. It was a surprising finding that y_0 , y_m and K_m could be easily determined in the optimizations, but that high n values were very difficult, if possible, to determine accurately. Still, the fdao analysis provides an explanation to this as discussed in details in Section B.1 and is presented graphically in Figure 6 which shows that the contribution n to the residuals decreases as n grows, determining a minor role of n uncertainty in the optimization process (Figure 6D).

Sample theory states that estimates of parameters such as mean, variance, skewness and kurtosis, become less variable and converge towards population values as sample size grows [62]. Data in Tables 3 to 5 show that estimated Sk and Kr do not converge but grow with sample size. Lack of convergence of sample mean, variance, skewness and kurtosis for Cauchyan random variables reflects that there are no population parameters to converge towards.

The Hill equation is not always used to fit Cauchyan data. Many, if not most, of the situations where the Hill equation is fitted to data, are direct measurements of a drug effect, an enzyme cat-

alytic rate, or gas-metal surface interactions [18, 54, 55, 85–89]. Hence, no quotients are calculated, and there is no reason to deal with Cauchy random variables. Results of fitting Gaussian data to the modified Hill equation are shown in Tables 6 to 8. As seen in Tables 6 to 8 even though the data submitted to the simplex optimization were Gaussian, all parameter estimates in the tables are leptokurtic and somewhat skewed, to a degree that all of them tested non-Gaussian with the Jarque-Bera and Shapiro-Wilk tests [41, 42]. Some of the parameter ranges were quite wide. Still, in contrast with data in Tables 3 to 5, neither Sk nor Kr seem to depend on sample sizes in Tables 6 to 8, which suggests that, whichever their distribution, their central moments are defined, and their sample estimates converge towards population values as sample size grows.

A function also subjected to fdao analysis (Section 3.3.1) was the Boltzmann distribution function [Eq. (48), revised in [77]]. Data in Tables 9 and 10 shows considerable independence between initial and predicted ($\{\theta\}$, Section 1), and sample size (r) values. in agreement with the discussion of Eqs. (49) and (50) and Figure 7. Predicted parameters were also leptokurtic. their distribution had low Sk , and Sk and Kr values seemed independent from sample sizes (r) and $\{\theta\}_{init}$. Ranges of predicted parameters were quite narrow. Thus, the Boltzmann function seems easier to optimize to the correct parameter values than the Hill equation [Eq. (24)]. This agrees with the fdao analysis done in Sections B.1 and C.1.

5. Appendices

A. The Hessian matrix

The *Hessian* matrix of a function $y(x_j | \{\theta\})$ is a matrix of second partial derivatives of the form

$$\mathbf{H}f[y(x | \{\theta\})] = \begin{bmatrix} \frac{\partial^2 y(x | \{\theta\})}{\partial \theta_1^2} & \frac{\partial^2 y(x | \{\theta\})}{\partial \theta_1 \partial \theta_2} & \frac{\partial^2 y(x | \{\theta\})}{\partial \theta_1 \partial \theta_3} & \frac{\partial^2 y(x | \{\theta\})}{\partial \theta_1 \partial \theta_4} \\ \frac{\partial^2 f(y(x | \{\theta\}))}{\partial \theta_2 \partial \theta_1} & \frac{\partial^2 y(x | \{\theta\})}{\partial \theta_2^2} & \frac{\partial^2 f(y(x | \{\theta\}))}{\partial \theta_2 \partial \theta_3} & \frac{\partial^2 y(x | \{\theta\})}{\partial \theta_2 \partial \theta_4} \\ \frac{\partial^2 f(y(x | \{\theta\}))}{\partial \theta_3 \partial \theta_1} & \frac{\partial^2 f(y(x | \{\theta\}))}{\partial \theta_3 \partial \theta_2} & \frac{\partial^2 y(x | \{\theta\})}{\partial \theta_3^2} & \frac{\partial^2 f(y(x | \{\theta\}))}{\partial \theta_3 \partial \theta_4} \\ \frac{\partial^2 y(x | \{\theta\})}{\partial \theta_4 \partial \theta_1} & \frac{\partial^2 y(x | \{\theta\})}{\partial \theta_4 \partial \theta_2} & \frac{\partial^2 y(x | \{\theta\})}{\partial \theta_4 \partial \theta_3} & \frac{\partial^2 y(x | \{\theta\})}{\partial \theta_4^2} \end{bmatrix} \quad (39)$$

where $x_j = [D_j]$ and $\{\theta\} = \{y_0, y_m, K_m, n\}$ for Equation (24). If $\{\theta\}$ are all linearly independent, then $Hf(y(x | \{\theta\}))$ is the *diagonal* matrix:

$$\mathbf{H}^L f[y(x | \{\theta\})] = \begin{bmatrix} \frac{\partial^2 y(x | \{\theta\})}{\partial \theta_1^2} & 0 & \dots & 0 \\ 0 & \frac{\partial^2 y(x | \{\theta\})}{\partial \theta_2^2} & \dots & 0 \\ \vdots & \vdots & \ddots & \vdots \\ 0 & 0 & \dots & \frac{\partial^2 y(x | \{\theta\})}{\partial \theta_n^2} \end{bmatrix}$$

B. Case study one: A modified Hill equation, or the Hill equation with offset

B.1. Modified Hill equation first derivatives at an optimum in presence of uncertainty

Equation (24) has the following first derivatives:

$$\omega(y_0) = \frac{\partial y([D] \mid \{\theta_i\})}{\partial y_0} = 1 \quad (40)$$

$$\omega(y_m) = \frac{\partial y([D] \mid \{\theta_i\})}{\partial y_m} = \frac{1}{1 + \zeta} \quad (41)$$

$$\omega(K_m) = \frac{\partial y([D] \mid \{\theta_i\})}{\partial K_m} = -\frac{\zeta \cdot n \cdot y_m}{K_m \cdot (1 + \zeta)^2} \quad (42)$$

$$\omega(n) = \frac{\partial y([D] \mid \{\theta_i\})}{\partial n} = -\frac{\zeta \cdot y_m \cdot \log(\zeta)}{n \cdot (1 + \zeta)^2}, \quad (43)$$

where $\zeta = \left(\frac{K_m}{[D]}\right)^n$.

Figure 6 presents plots of Eqs. (40) through (43) as functions of $[D]$. To simplify comprehension, absolute values of the derivatives are plotted, please notice that Eqs. (42) and (43) have negative signs. Parameters used to calculate the derivatives in Figure 6 were $\{y_0 = -0.1, y_m = 1, K_m = 0.5, n = 1, 2, 3 \text{ or } 10\}$. Numbers near the curves indicate the value of n used to calculate each curve. Eq. (40) tells that $\omega(y_0)$ is constant for any $[D]$, but the other derivatives are more sophisticated functions of $[D]$. Next, $\omega(y_m) = 0$ when $[D]=0$, grows with $[D]$ and becomes increasingly sigmoid as n increases, all curves describing $\omega(y_m)$ intercept at $[D] = K_m$, at this point the curves increase in slope as n increases, and

$$\left[\lim_{[D] \rightarrow +\infty} \omega(y_m) = 1 \right] \forall (K_m \wedge n) \in (0, +\infty),$$

and in all cases $\omega(y_m) = 0.5 \implies [D] = K_m$. Also,

$$\{([D] = 0) \vee ([D] = +\infty)\} \forall (n \geq 0) \in \mathbb{R} \implies \omega(K_m) = 0$$

and

$$\{([D] = K_m) \vee (n \geq 0) \in \mathbb{R}\} \implies \max[\omega(K_m)].$$

In contrast with Eqs. (40) through (42), Eq. (43) has tree roots and two maxima, one below and one above K_m , and this relation holds:

$$\{([D] = 0) \vee ([D] = K_m) \vee ([D] = \infty)\} \forall (n \geq 0) \in \mathbb{R} \implies \omega(n) = 0.$$

There is another difference between $\omega(n)$ and the other three derivatives: $\lim_{n \rightarrow +\infty} |\omega(n)| = 0$, the bigger n gets, the least it contributes to $y([D] \mid \{\theta\})$ uncertainty, making it harder to guess in any optimization procedure when $n \gg 1$ since there is less and less to minimize in regard to n as it increases. With the same reasoning since

$$\{|\omega(y_0)| > |\omega(y_m)|\} \forall [D]$$

it would be easier to determine y_0 with more accuracy than y_m ; in colloquial terms y_0 introduces the same uncertainty over all the $[D]$ range, while y_m contribution increases with $[D]$. Data in Figure 6 suggest also that accuracy of K_m is higher if n is higher and when enough data is collected around K_m .

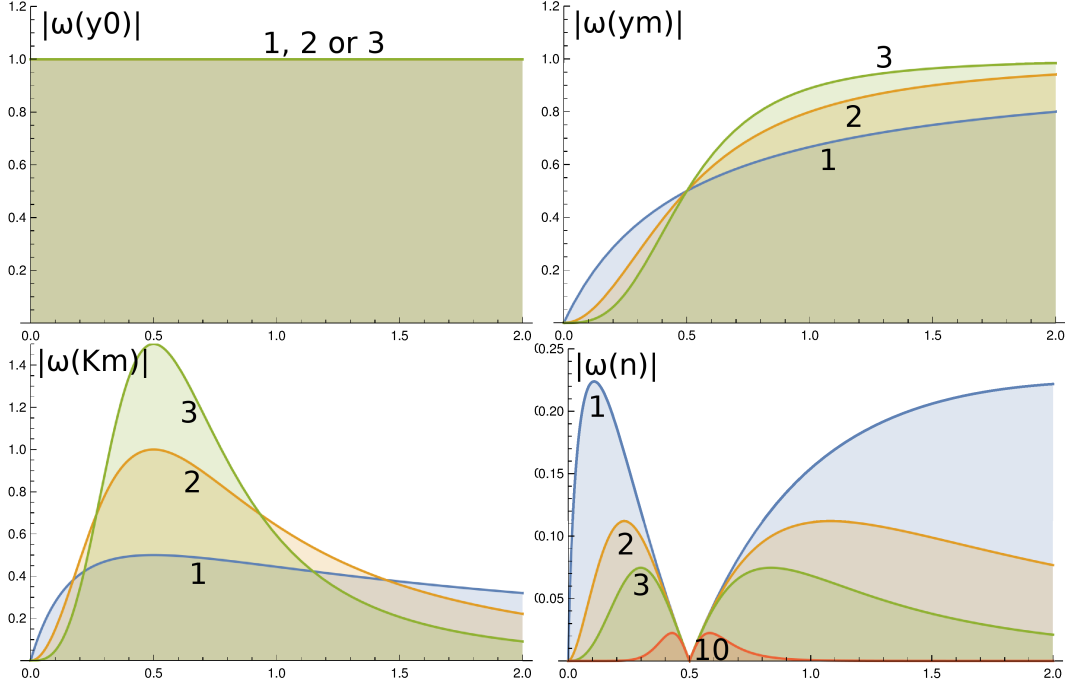


Figure 6: $y([D] | \{\theta\})$ rate of change absolute value as function of y_0 , y_m , K_m , and n . Parameters used to calculate the derivatives were $\{y_0 = -0.1, y_m = 1, K_m = 0.5, n = 1, 2 \text{ and } 3\}$ except for $\omega(n)$ where $n = 1, 2, 3$ and 10 . Lettering in the panels indicate: $|\omega(y_0)| = \omega(y_0)$ absolute value calculated with Eq. (40); $|\omega(y_m)| = \omega(y_m)$ absolute value calculated with Eq. (41); $|\omega(K_m)| = \omega(K_m)$ absolute value calculated with Eq. (42) and $|\omega(\mathbf{n})| = \omega(\mathbf{n})$ absolute value calculated with Eq. (43). Numbers near the curves indicate the value of n used to calculate each curve. Please notice that the abscissa has same value in all panels, top panels have the same ordinate scale, but lower panels have different ordinate scales between them, and also different from the top panels. Other details in the text of the communication.

The most uncertain parameter to estimate seems to be n , data in Figure 6 suggests, however that accuracy of n estimates improve when data between $\frac{1}{2}K_m$ and $2K_m$ is more available, but that even then a good estimate of a high n would be difficult (if possible) to get, as it is suggested by the curve calculated setting $n = 10$.

B.2. The modified Hill equation Hessian matrix.

The Hessian matrix, of Eq. (24) is the *nondiagonal* matrix:

$$Hy([D] | \{\theta\}) = \Xi \cdot \begin{bmatrix} 0 & 0 & 0 & 0 \\ 0 & 0 & -\frac{n}{K_m} & -\frac{\log(\zeta)}{n} \\ 0 & 0 & \frac{n[\zeta+(\zeta-1)n+1]y_m}{K_m^2(\zeta+1)} & -\frac{y_m[\zeta-(\zeta-1)\log(\zeta)-1]}{K_m(\zeta+1)} \\ 0 & -\frac{\log(\zeta)}{n} & -\frac{y_m[\zeta-(\zeta-1)\log(\zeta)-1]}{K_m(\zeta+1)} & \frac{(\zeta-1)y_m \log^2(\zeta)}{n^2(\zeta+1)} \end{bmatrix} \quad (44)$$

where

$$\Xi = \frac{\zeta}{(1+\zeta)^2}. \quad (45)$$

Equation(44) shows the Hill equation nonlinearity, Also if $[D] = K_m$ then $\Xi = \frac{1}{4}$ and

$$\text{Hy}([D] = K_m \mid \{\theta\}) = \frac{y_m}{4K_m} \cdot \begin{bmatrix} 0 & 0 & 0 & 0 \\ 0 & 0 & -\frac{n}{y_m} & 0 \\ 0 & 0 & \frac{n}{K_m} & -1 \\ 0 & 0 & -1 & 0 \end{bmatrix} \quad (46)$$

where $\left\{0, 0, \frac{(n-\sqrt{4K_m^2+n^2})y_m}{8K_m^2}, \frac{(n+\sqrt{4K_m^2+n^2})y_m}{8K_m^2}\right\}$ are the eigenvalues of $\text{Hy}([D] = K_m \mid \{\theta\})$, and

$$\text{Disc} \{ \text{Hy}([D] = K_m \mid \{\theta\}) \} = \frac{y_m}{4K_m} \begin{pmatrix} 0 & 0 & 0 & 0 \\ 0 & 0 & -\frac{n}{y_m} & 0 \\ 0 & 0 & \frac{n}{K_m} & -1 \\ 0 & 0 & -1 & 0 \end{pmatrix} = 0 \quad (47)$$

where Disc stands for *Discriminant*, a determinant form of the Hessian matrix. Since Disc = 0 when $[D] = K_m$ the function reaches a *degenerate critical point* [90] where $y([D] \mid \{\theta\})$ has an inflection.

C. Case study two: The Boltzmann equation.

A common form of the Boltzmann equation used in biology is [77]:

$$B(V \mid \{V_{\frac{1}{2}}, \kappa\}) = \frac{1}{1 + e^{-(V-V_{\frac{1}{2}})/\kappa}}. \quad (48)$$

When Eq. (48) is used in the original fashion of Hodgkin and Huxley [78, pg 501, Eq. 1], to represent trans membrane distribution of some charged particle, B is expressed in respect to the potential at which 50% of the particles are in one side of the membrane, and 50% is at the other side. Eq. (48) is thus reduced to a situation where a dependent variable B may be fitted by some nonlinear optimization procedure to an independent variable V (usually expressed in mV) using Eq. (48). The optimization procedure enables to estimate the parameters $V_{\frac{1}{2}}$ and κ .

C.1. Boltzmann equation first derivatives at an optimum in presence of uncertainty.

Mathematical properties of the Boltzmann equation are discussed elsewhere [77]. But since the first derivatives of Eq. (48) respect to $\{\theta_i\}$ are crucial for this paper, they are presented here:

$$\omega(V_{\frac{1}{2}}) = \frac{\partial B(V \mid V_{\frac{1}{2}}, \kappa)}{\partial V_{\frac{1}{2}}} = -\frac{1}{2\kappa \cosh\left(\frac{\varpi}{\kappa}\right) + 2\kappa} \quad (49)$$

$$\omega(\kappa) = \frac{\partial B(V \mid V_{\frac{1}{2}}, \kappa)}{\partial \kappa} = -\frac{\varpi \operatorname{sech}^2\left(\frac{\varpi}{2\kappa}\right)}{4\kappa^2} \quad (50)$$

where $\varpi = V - V_{\frac{1}{2}}$. Eqs. (49) and (50) contrast sharply with the situation discussed in connection with Eqs. (40) through (43), Even though Eq. (49) reaches a maximum while Eq. (50) reaches a

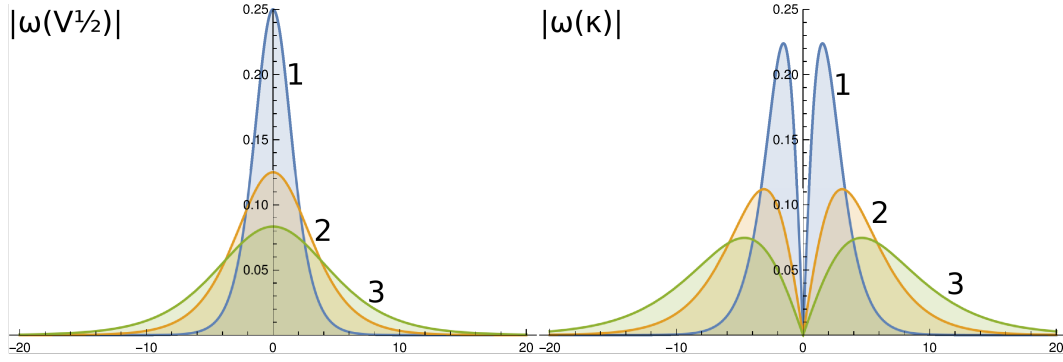


Figure 7: $\mathbf{B}(V | V_{\frac{1}{2}}, \kappa)$ rate of change absolute value as function of $V_{\frac{1}{2}}$, and κ . Parameters used to calculate the derivatives were $V_{\frac{1}{2}} = 0$ and $\kappa = 1, 2$ and 3 . Lettering in the panels indicate: $|\omega(V^{1/2})| = \omega(V_{\frac{1}{2}})$ absolute value calculated with Eq. (49); $|\omega(\kappa)| = \omega(\kappa)$ absolute value calculated with Eq. (50). Numbers near the curves indicate the value of κ used to calculate each curve. Other details in the text of the communication.

minimum at K_m , in the vicinity of this value the two derivatives have similar high values which grow as κ gets higher and $|V| \rightarrow +\infty$, this suggests that both parameters contribute similar uncertainties to random variables distributed around $B(V | \{V_{\frac{1}{2}}, \kappa\})$ and that that both $V_{\frac{1}{2}}$ and κ will be determined with similar accuracies after optimization.

C.2. Boltzmann equation gradient

$$\nabla B(V | \{V_{\frac{1}{2}}, \kappa\}) = -\frac{(\kappa + \varpi) \operatorname{sech}^2\left(\frac{\varpi}{2\kappa}\right)}{4\kappa^2} \quad (51)$$

if $\varpi = 0$ then

$$\nabla B(V = V_{\frac{1}{2}} | \{V_{\frac{1}{2}}, \kappa\}) = -\frac{1}{4\kappa} \quad (52)$$

which shows that the gradient at ϖ only depends on κ .

Conflicts of interests

There are no conflicts of interest. But it seems fair to state that starting from April 2018, C. Sevcik is the CEO of SciMeDan (www.scimedan.com, blogg.scimedan.com) a group dedicated to statistical, clinical studies and pharmacokinetics counseling.

Acknowledgments

This manuscript was written in L^AT_EX using *T_EXstudio* v. 2.12.8 for Linux (Also available for Apple OS X and MS Windows, <http://www.texstudio.org>), an open source free T_EX editor.

References

References

- [1] D. C. Montgomery, E. A. Peck, and G. G. Vining. Introduction to Linear Regression Analysis. John Wiley and Sons, Inc., 5 edition, June 2015.

- [2] G.A. Seber and C.J. Wild. Nonlinear Regression. John Wiley & Sons, New York, 1989.
- [3] K. Schittkowski. Numerical Data Fitting in Dynamical Systems. A Practical Introduction with Applications and Software, volume 77 of Applied Optimization. Kluwer Academic Publishers, Boston, MA, 2002.
- [4] W. Heisenberg. Über den anschaulichen inhalt der quantentheoretischen kinematik und mechanik. Zeit. Physik, 43:172–198, 1927.
- [5] M. Sassoli de Bianchi. The observer effect. Found. Sci., 18:213–243, 2013.
- [6] M. Conrad. Functional significance of biological variability. Bul. Math. Biol., 39:139–156, 1977. doi: 10.1007/BF02462854.
- [7] J. Gilluly. Distribution of mountain building in geologic time. Bull. Geol. Soc. Am., 60: 661–690, 1949.
- [8] J. Evans. How high is Mont Blanc? Chamonix High Mountain Reporter, September 8th 2015.
- [9] P. M. A. Sherwood. Vibrational Spectroscopy of Solids. Cambridge University Press, Cambridge, UK, 1972.
- [10] P. Mörters. Random fractals. In W. Kndall and Y. S. Molhanov, editors, New Perspectives in Stochastic Geometry, chapter 8. Oxford University Press, Oxford, UK, 2009.
- [11] P. Mörters and Y. Peres. Brownian Motion, volume 30. Cambridge University Press, Cambridge, UK, 2010.
- [12] The CMS Collaboration. Precise determination of the mass of the Higgs boson and tests of compatibility of its couplings with the standard model predictions using proton collisions at 7 and 8 TeV, January 2015. URL arxiv.org/pdf/1412.8662.pdf. European Organization for Nuclear Research (CERN) CERN-PH-/2013-037 2015/06/16.
- [13] J Del Castillo and B. Katz. The effect of magnesium on the activity of motor nerve endings. J. Physiol., 124:553–559, 1954.
- [14] C. M. Armstrong and F. Bezanilla. Charge movement associated with the opening and closing of the activation gates of the Na channels. J. Gen. Physiol., 63:533–552, 1974.
- [15] H. M. Fishman, D. J. M. Poussart, and L. E. Moore. Noise measurements in squid axon membrane. J. Memb. Biol., 24:281–304, 1975.
- [16] E. Neher and B. Sakmann. Single-channel currents recorded from membrane of denervated frog muscle fibres. Nature, 260:799–802, 1976.
- [17] E. J. Ariëns, A. M. Simonis, and J. M. Van Rossum. Molecular pharmacology. The mode of action of biologically active compounds, volume 1 of Medicinal Chemistry, chapter Drug-receptor interaction: Interaction of one or more drugs with one reeptor system, pages 119–286. Academic Press, New York, 1964.

- [18] I. H. Segel. Enzyme Kinetics. Wiley-Interscience, New York, 1975.
- [19] P. Érdi and J. Tóth. Mathematical Models of Chemical Reactions: Theory and Applications of Deterministic and Stochastic Models. Manchester University Press, Manchester, UK, 1989. ISBN 978-0-7190-2208-1.
- [20] R. V. Hogg and A. T. Craig. Introduction to mathematical statistics. Macmillan Publishing Co., Inc., London, UK, 4 edition, 1978.
- [21] W. Spohn. Stochastic independence, causal independence, and shieldability. J. Phil. Logic, 9:73–99, 1980.
- [22] A. B. Ghorbal and M. Schürman. Non-commutative notions of stochastic independence. Math. Proc. Cambr. Phil. Soc., 133:531–561, 2002.
- [23] M. Lostaglio and M. P. Müller and M. Pastena. Stochastic independence as a resource in small-scale thermodynamics. [arXiv:1409.3258v4](https://arxiv.org/abs/1409.3258v4), October 2015.
- [24] M. Lostaglio, M. P. Müller, and M. Pastena. Stochastic independence as a resource in small-scale thermodynamics. Phys. Rev. Lett., 115:150402–1–150402–5, 2015.
- [25] J. Goold, M. Huber, A. Riera, L. del Rio, and P. Skrzypczyk. The role of quantum information in thermodynamics—a topical review. J. Phys. A: Math. Theor., 49:1–50, 2016. doi: 10.1088/1751-8113/49/14/143001.
- [26] E. W. Weisstein. Minkowski sum, 2018. URL <http://mathworld.wolfram.com/MinkowskiSum.html>.
- [27] H. Cramér. Mathematical Methods of Statistics. Princeton, 18 edition, 1991.
- [28] J. Pitman. Probability. Springer Texts in Statistics. Springer Verlag, New York, 1 edition, 1993.
- [29] S. Wolfram. The Mathematica[®] Book. Wolfram Media, Champaign, IL, 5 edition, 2003.
- [30] L. Boltzmann. Vorlesungen über Gastheorie, volume 1. Barth, Leipzig, 1896.
- [31] L. Boltzmann. Lectures on gas theory. University of California Press–Dover, Berkeley–New York, 1964. Translated by Stephen G. Brush.
- [32] G. Dahlquist and Å. Björk. Numerical Methods. Prentice Hall Inc., Englewood Cliffs, 1974.
- [33] G. E. P. Box and M. E. Muller. A note on the generation of random normal deviates. Ann. Math. Stat., 22:610–611, 1958.
- [34] W. H. Press, S. A. Teukolsky, W. T. Vetterling, and B. P. Flannery. Numerical Recipes in C. The Art of Scientific Computing. Cambridge University Press, Cambridge, England, 1992.
- [35] M. Matsumoto and T. Nishimura. Mersenne twister: A 623-dimensionally equidistributed uniform pseudorandom number generator. ACM Trans. Mod. Com. Sim., 8:3–30, 1998.

- [36] F. O. Panneton, P. l'Ecuyer, and M. Matsumoto. Improved long-period generators based on linear recurrences modulo 2. ACM Trans. Mathem. Softw., 32:1–16, 2006.
- [37] G. Marsaglia, W. W. Tsang, and J. Wang. Evaluating Kolmogorov's distribution. J. Stat. Soft., 8:1–4, 2003.
- [38] J. Bellamy. Randomness of D sequences via diehard testing. <http://arxiv.org/abs/1312.3618>, Dec 2013.
- [39] J. Nelder and R. Mead. A simplex method for function minimization. Comp. J., 7:308–313, 1965.
- [40] F. E. Grubbs. Procedures for detecting outlying observations in samples. Technometrics, 11: 1–21, 1969.
- [41] A. K. Bera and C. M. Jarque. Efficient tests for normality, homoscedasticity and serial independence of regression residuals: Monte Carlo evidence. Econ. Lett., 7:313–318, 1981.
- [42] S. S. Shapiro and M. B. Wilk. An analysis of variance test for normality (complete samples). Biometrika, 52:591–611, 1965.
- [43] M. Hollander and D. A. Wolfe. Nonparametric statistical procedures. Wiley, New York, 1973.
- [44] R. A. Quintana-Hernández. Evaluación de la actividad citotóxica de la ascidia *Polyclinum constellatum* (Savigny, 1816) y su posible efecto sobre la línea celular de cancer de mama (4T1). Trabajo de Grado para optar a la Licenciatura en Biología Marina, Universidad De Oriente Núcleo Nueva Esparta. Escuela De Ciencias Aplicadas Del Mar, Boca del Río, Nueva Esparta, Venezuela, Diciembre 2017.
- [45] T.F.Slater, B. Sawyer, and U. Sträuli. Sstudies on succinate-tetrazolium reductas III. Points of coupling of four different tetrazolium salts. Bioch. Biophys. Acta, 77:383–393, 1963.
- [46] T. Mosmann. Rapid colorimetric assay for cellular growth and survival: application to proliferation and cytotoxicity assays. J. Immun. Methods, 65:55–63, 1983.
- [47] F. Denizot and R. Lang. Rapid colorimetric assay for cell growth and survival: Modifications to the tetrazolium dye procedure giving improved sensitivity and reliability. J. Immunol. Methods, 89:271–277, 1986.
- [48] D. F. Swinehart. The Beer-Lambert law. J. Chem. Edu., 39:333–335, 1962.
- [49] J. L. Hodges, Jr. and E. L. Lehmann. Estimates of location based on rank tests. Ann. Math. Stat., 34:598–611, 1963. doi: 10.1214/aoms/1177704172.
- [50] W. Kahan. Pracniques: further remarks on reducing truncation errors. Comm. ACM, 8: 40–41, 1964.
- [51] W. Kahan. On the cost of floating-point computation without extra-precise arithmetic. Internet, November 2004. URL people.eecs.berkeley.edu/~wkahan/Qdrtcs.pdf.

- [52] S. Boldo and C. Marché. Formal verification of numerical programs: From c annotated programs to mechanical proofs. Mathematics in Computer Science, 5:377–393, Dec 2011. doi: 10.1007/s11786-011-0099-9.
- [53] J-O. Rawlings, S. G. Pantula, and D. A. Dickey. Applied Regression Analysis: A Research Tool. Springer Texts in Statistics. Springer, New York, USA, 2 edition, 1998.
- [54] A. V. Hill. The possible effects of the aggregation of the molecules of haemoglobin on its dissociation curves. J. Physiol. (Lond.), 40(Proceedings):iv–vii, 1910.
- [55] A. V. Hill. The combinations of haemoglobin with oxygen and with carbon monoxide. I. Bioch. J., 7:471–480, 1913.
- [56] J. Monod, J. Wyman, and J.-P. Changeux. On the nature of allosteric transitions: a plausible model. J. Mol. Biol., 12:88–118, 1965.
- [57] H. Abeliovich. An empirical extremum principle for the Hill coefficient in ligand-protein interactions showing negative cooperativity. Bioph. J., 89:76–79, 2005.
- [58] R. J. LeVeque. Finite difference methods for differential equations. Class notes for AMath 585–6, University of Washington, 1998. URL www.rsmas.miami.edu/users/miskandarani/Courses/MSC321/lectfiniteDifference.pdf.
- [59] T. J. Rothenberg, F. M. Fisher, and C. B. Tilanus. A note on estimation from a Cauchy sample. J. Ame. Stat. Assoc., 59(306):460–463, 1964.
- [60] E. F. Fama and R. Roll. Some properties of symmetric stable distributions. J. Am. Stat. Assoc., 63:817–836, 1968.
- [61] H. Lohninger. Fundamentals of statistics. http://www.statistics4u.info/fundstat_eng/ee_distri_cauchy.html, November 2012. Epina e-Book.
- [62] S. S. Wilks. Mathematical Statistics. Wiley, New York, 1962.
- [63] G. R. Shorack and J. A. Wellner. Empirical processes with applications to statistics. Wiley, New York, 1986.
- [64] K Pearson. Contributions to the mathematical theory of evolution. I. Phil. Trans. Roy. Soc. Lond. Ser. A, 185:71–110, 1894.
- [65] E. S. Pearsons. Some problems arising in approximating to probability distributions, using moments. Biometrika, 50:95–112, 1963.
- [66] K. Pearson. “Das Fehlergesetz und Seine Verallgemeinerungen Durch Fechner und Pearson.”. A rejoinder. Biometrika, 4:169–212, 1905.
- [67] L. Faleschini. Su alcune proprietà dei momenti impiegati nello studio della variabilità, asimmetria e curtosi. Statistica, 8:503–513, 1948.

- [68] F. Proschan. Peakedness of distributions of convex combinations. Ann. Math. Stat., 36: 1703–1706, 1965.
- [69] R. B. Darlington. Is kurtosis really ‘peakedness’? American. Stat., 24, 1970.
- [70] D. K. Hildebrand. Kurtosis measures bimodality? Am. Stat., 25, 1971.
- [71] M. M. Ali. Stochastic ordering and kurtosis measure. J. Am. Stat. Assoc., 69:543–545, 1974.
- [72] M. E. Johnson, G. L. Tietjen, and R. J. Beckman. A new family of probability distributions with applications to Monte Carlo studies. J. Am. Stat. Assoc., 75:276–279, 1980.
- [73] J. J. A. Moors. The meaning of kurtosis: Darlington reexamined. Am. Stat., 40, 1986.
- [74] D. Ruppert. What is kurtosis? an influence function approach. Am. Stat., 41, 1987.
- [75] H. Westfall. Kurtosis as peakedness, 1905 – 2014. *R.I.P.* Am. Stat., 68:191–195, 2014.
- [76] L. T. DeCarlo. On the meaning and use of kurtosis. Psychol, Methods, 2:292–307, 1997.
- [77] C. Sevcik. Caveat on the Boltzmann distribution function use in biology. Prog. Bioph. Mol. Biol., 127:33–42, 2017. doi: 10.1016/j.pbiomolbio.2017.04.003.
- [78] A. L. Hodgkin and A. F. Huxley. A quantitative description of membrane current and its application to conduction and excitation in nerve. J. Physiol., 117:500–544, 1952.
- [79] S. Peigneur, C. Sevcik, J. Tytgat, C. Castillo, and G. D’Suze. Subtype specificity interaction of baxtridines with mammalian, insect and bacterial sodium channels under voltage clamp conditions. FEBS J., 279:4025–4038, 2012.
- [80] J. A. Cadzow. Minimum ℓ_1 , ℓ_2 , and ℓ_∞ Norm approximate solutions to an overdetermined system of linear equations. Dig. Sign. Proces., 12:524—560, 2002.
- [81] D. L. Donoho. For most large underdetermined systems of linear equations the minimal ℓ_1 -norm solution is also the sparsest solution. Comm. Pure App.Math., 59:797–829, 2006.
- [82] L. E. Ballentine. The statistical interpretation of quantum mechanics. Rev. Mod. Phys., 12: 358–381, 1970.
- [83] G. J. Augustine and H. Kasai. Bernard Katz, quantal transmitter release and the foundations of presynaptic physiology. J. Physiol., 578:623–625, 2007.
- [84] J. Cronin. Mathematical aspects of Hodgkin-Huxley neural theory. Cambridge University Press, Cambridge, UK, 1987.
- [85] J. Barcroft and A. V. Hill. The nature of oxyhaemoglobin, with a note on its molecular weight. J. physiol., 39:411–428, 1910.
- [86] I. Langmuir. The adsorption of gases on plane surfaces of glass, mica and platinum. J. Am. Chem. Soc., 40:1361–1403, 1918.

- [87] J N Weiss. The Hill equation revisited: uses and misuses. FASEB J-, 11:835–841, 1997.
- [88] R. Gesztelyi, J. Zsuga, A. Kemeny-Beke, B. Varga, B. Juhasz, and A. Tosaki. The Hill equation and the origin of quantitative pharmacology. Arch. Hist. Exact Sci., 66:427–438, 2012.
- [89] R. Reeve and J. R. Turner. Pharmacodynamic models: Parameterizing the Hill equation, michaelis-menten, the logistic curve, and relationships among these models. J. Biopharm. Stat., 23:648–661, 2013.
- [90] T. S. Bolis. Degenerate critical points. Mathem. Magaz., 53:294–299, 1980.